SANDIA REPORT
SAND2020-10779
Printed October 2020

Sandia National Laboratories

Radar Motion Measurements and Synthetic Aperture Radar Image Geolocation Accuracy

Armin W Doerry and Douglas L Bickel

Prepared by
Sandia National Laboratories
Albuquerque, New Mexico
87185 and Livermore,
California 94550

Issued by Sandia National Laboratories, operated for the United States Department of Energy by National Technology & Engineering Solutions of Sandia, LLC.

Available to DOE and DOE contractors from
U.S. Department of Energy
Office of Scientific and Technical Information
P.O. Box 62
Oak Ridge, TN 37831

Telephone: (865) 576-8401
Facsimile: (865) 576-5728
E-Mail: reports@osti.gov
Online ordering: http://www.osti.gov/scitech

Available to the public from
U.S. Department of Commerce
National Technical Information Service
5301 Shawnee Rd
Alexandria, VA 22312

Telephone: (800) 553-6847
Facsimile: (703) 605-6900
E-Mail: orders@ntis.gov
Online order: https://classic.ntis.gov/help/order-methods/

Radar Motion Measurements and Synthetic Aperture Radar Image Geolocation Accuracy

Armin W Doerry and Douglas L Bickel

Abstract

Once a Synthetic Aperture Radar (SAR) image is formed, the natural question then is “Where is this image?” and/or “Where exactly is this feature displayed in the image?” Thus, geolocation is an important exploitation of the SAR image. Since SAR measures relative location to its own position, it is crucial to understand how the radar’s position and motion impacts the ability to geolocate a feature in the SAR image. Furthermore, accuracy and precision of navigation aids like GPS directly impact the goodness of the geolocation solution. These relationships are developed and discussed.

Acknowledgements

This report was funded by General Atomics Aeronautical Systems, Inc. (GA-ASI) Mission Systems under Cooperative Research and Development Agreement (CRADA) SC08/01749 between Sandia National Laboratories and GA-ASI.

General Atomics Aeronautical Systems, Inc. (GA-ASI), an affiliate of privately-held General Atomics, is a leading manufacturer of Remotely Piloted Aircraft (RPA) systems, radars, and electro-optic and related mission systems, including the Predator®/Gray Eagle®-series and Lynx® Multi-mode Radar.

We offer a special thanks to our colleague Scott Jenkins for his comments on motion measurement instruments, techniques, and performance. In addition, we are very grateful to William “Hutch” Hutcheson of General Atomics, ASI, for stimulating and enlightening discussions on motion measurement and related topics.

Contents

List of Figures

List of Tables

"Before I speak, I have something important to say."
-- Groucho Marx

Acronyms and Definitions

1-D, 2-D, 3-D	1-, 2-, 3-Dimesional
APC	Antenna Phase Center
AWGN	Additive White Gaussian Noise
C/A	Coarse Acquisition
CDF	Cumulative Density Function
CEP	Circular Error Probability
DEM	Digital Elevation Model/Map
DGPS	Differential-GPS
DTED	Digital Terrain Elevation Data
EKF	Extended Kalman Filter
EM	Electromagnetic
FAA	Federal Aviation Administration
GNSS	Global Navigation Satellite System
GPS	Global Positioning System
HRE	High Resolution Elevation
HRTE	High-Resolution Terrain Information
IMU	Inertial Measurement Unit
IPR	Impulse Response
KF	Kalman Filter
L1	1575.42 MHz frequency band of GPS
MIG	Multiple-Image Geopositioning
NGA	National Geospatial-Intelligence Agency
PPM	Parts Per Million
PDF	Probability Density Function
PSD	Power Spectral Density
RMS	Root Mean Square
RX	Receive or Receiver
SAR	Synthetic Aperture Radar
SIG	Single-Image Geopositioning
SNR	Signal to Noise Ratio
SRP	Scene Reference Point
SRTM	Shuttle Radar Topography Mission
TX	Transmit or Transmitter
USGS	US Geological Service
UT-Austin	University of Texas at Austin
WAAS	Wide Area Augmentation System

Foreword

This report details the results of an academic study. It does not presently exemplify any modes, methodologies, or techniques employed by any operational system known to the authors.

Classification

The specific mathematics and algorithms presented herein do not bear any release restrictions or distribution limitations.

This report formalizes preexisting informal notes and other documentation on the subject matter herein.

This report is Unclassified, Unlimited Release.

Author Contact Information

Armin Doerry	awdoerr@sandia.gov	505-845-8165
Doug Bickel	dlbicke@sandia.gov	505-845-9038

1 Introduction

Synthetic Aperture Radar (SAR) is an imaging technique whereby maps of radar reflectivity are made from radar echo soundings along some flight path. The utility of the SAR mage is considerably enhanced with accurate and precise geolocation of the image.

Since radar makes relative measurements from its own position, i.e. the positions of its pulses along its flight path, the goodness of a SAR image's geolocation depends on the goodness of the geolocation of the radar from whence the pulses were sent and collected. Consequently, SAR image geolocation depends strongly on the radar's own motion measurement accuracy and precision.

A typical SAR motion measurement subsystem, often termed a "navigator," consists of an Inertial Measurement Unit (IMU) that is aided by a Global Navigation Satellite System (GNSS) such as the United States' Global Positioning System (GPS). The aiding is intended to keep the drift in the IMU's linear and angular motion bounded to within some acceptable limits. Consequently, the quality of a navigator's output will depend on the quality of the IMU instrument as well as the quality of the GNSS data. Alternatively, the required quality of the navigator's solution will flow to the required quality of the IMU and the GNSS instruments.

To be sure, SAR image geolocation will also depend on a number of factors other than the navigator solution, e.g. atmospherics dielectric properties, earth curvature, and scene topography, to name a few. However, in this report we restrict ourselves to the characteristics and nature of the navigator solution relevant to SAR image geolocation. In particular, we concern ourselves with geolocating a stationary retroreflector, or scattering point, in a conventional SAR image of stationary clutter.

These questions have been previously investigated by others, including presentation of a paper by Pedlar and Coe,[1] but herein we extend the results to farther ranges and longer-duration synthetic apertures.

"If you do not know where you are going, every road will get you nowhere."
-- Henry A. Kissinger

2 Background

Ultimately, we desire to assess the impact of navigator errors on SAR geolocation. We begin by examining error-free SAR operation, and then progress to including the effects of errors in the navigator. We take the liberty of referring to these scenarios as "Blue Pill" and "Red Pill" scenarios.[†]

2.1 Blue Pill

We begin with a model of geometric definitions relevant to our problem. Figure 1 illustrates the geometry of an error-free radar collection.

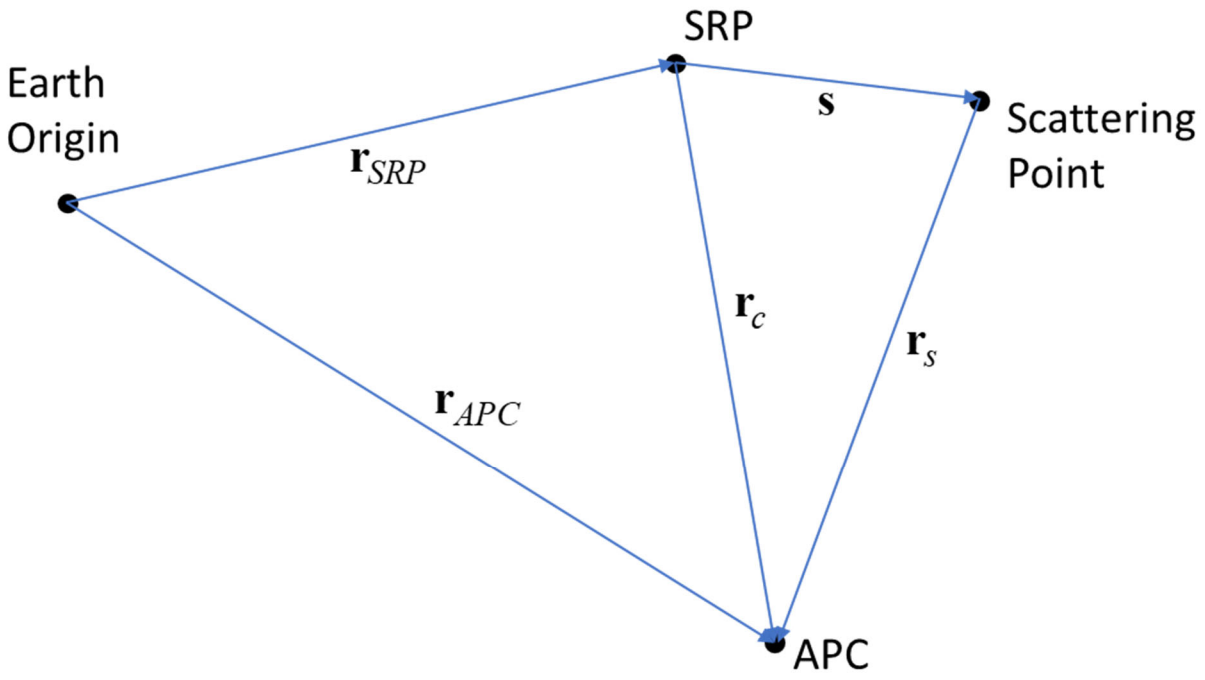

Figure 1. Geometry of error-free SAR data collection.

Relative to a fixed-earth coordinate frame, we define the following points.

Earth Origin = fixed-earth coordinate frame origin,
SRP = Scene Reference Point,
APC = Antenna Phase Center, and
Scattering Point = earth location we wish to geolocate. (1)

[†] In the 1999 science fiction motion picture *The Matrix* the principal character Neo is offered by rebel leader Morpheus a choice between returning to blissful ignorance in a simulated reality by taking a blue pill, or taking a red pill that would expose him to the discomfort of dealing with stark reality.

With these points so defined, we relate them to each other with the following vector definitions.

$\mathbf{r}_{SRP}$ = relative location of SRP from the Earth Origin,
$\mathbf{r}_{APC}$ = relative location of APC from Earth Origin,
$\mathbf{r}_c = \mathbf{r}_{APC} - \mathbf{r}_{SRP}$ = relative location of APC from SRP,
$\mathbf{s}$ = relative location of scattering point from SRP, and
$\mathbf{r}_s = \mathbf{r}_c - \mathbf{s}$ = relative location of APC from scattering point location. (2)

Of these,

$\mathbf{r}_{APC}$ is measured by the radar's navigator,
$\mathbf{r}_{SRP}$ is specified as an input to calculations,
$\mathbf{r}_c$ is calculated from navigation measurement data,
$|\mathbf{r}_s|$ is measured by radar echo soundings, and
$\mathbf{s}$ is calculated from a comparison of radar measurements to navigator calculations. (3)

Note that the radar echo soundings only measure the magnitude of the vector $\mathbf{r}_s$, and not its direction.

A synthetic aperture is generated by assembling a collection of radar echo soundings from different APC locations along a radar's flight path. This facilitates localizing echo energy to specific locations **s**.

Many SAR image formation algorithms exist to estimate energy at various scattering point locations, and hence to provide geolocated radar maps, generally employing approximations to matched filters, or more specifically correlation filters. The details of these are beyond the scope of this report.

At a high level, but sufficient for our purposes, we will assume the 2-D model in Figure 2. Accordingly, we define

(s_x, s_r) = coordinates for the scattering point location, assumed constants for SAR, and
$(v_x t, -r_{c0})$ = coordinates for the APC, which moves with time, (4)

where

v_x = cross-range velocity,
t = time referenced to the center of the synthetic aperture, and
r_{c0} = the scalar range from SRP to the APC at time $t = 0$. (5)

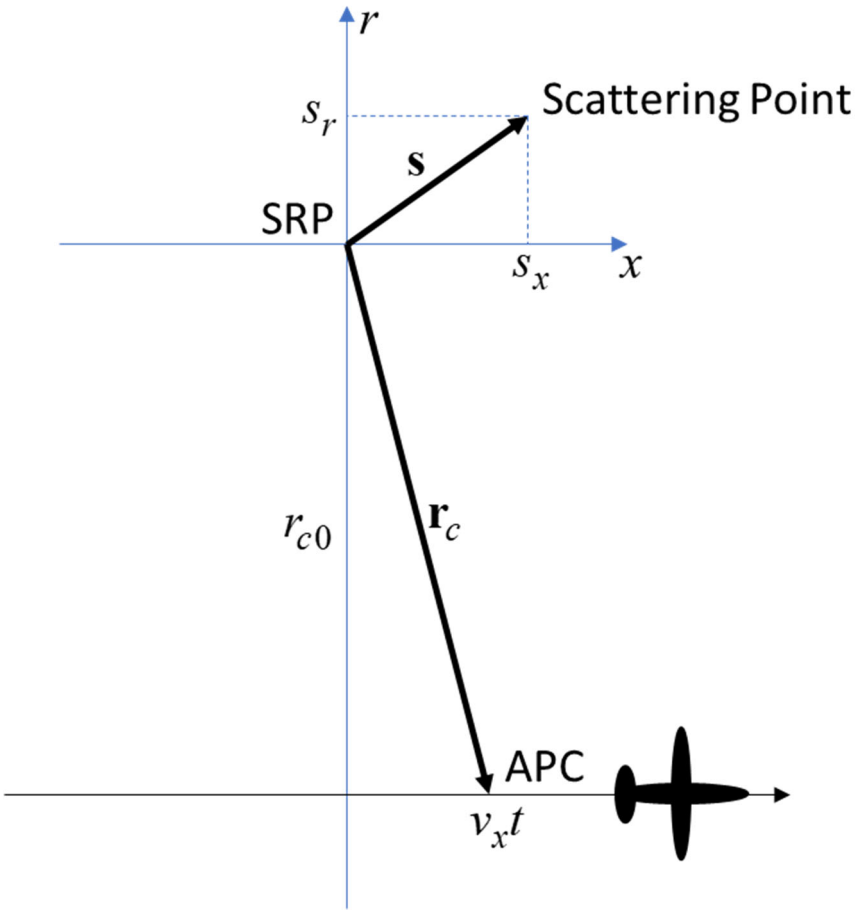

Figure 2. 2-D model with coordinate frame defined.

With these definitions, we identify

$$|\mathbf{r}_s| = |\mathbf{r}_c - \mathbf{s}| = \sqrt{(\mathbf{r}_c - \mathbf{s}) \bullet (\mathbf{r}_c - \mathbf{s})}, \tag{6}$$

which can be expanded to

$$|\mathbf{r}_s| = \sqrt{|\mathbf{r}_c|^2 + |\mathbf{s}|^2 - 2\mathbf{r}_c \bullet \mathbf{s}}\,. \tag{7}$$

We now identify coordinates for the various entities as

$$\begin{aligned} &\mathbf{r}_c \rightarrow (v_x t\,, -r_{c0}), \text{ and} \\ &\mathbf{s} \rightarrow (s_x\,, s_r)\,. \end{aligned} \tag{8}$$

We linearize $|\mathbf{r}_s|$ using a first-order Taylor series expansion about $t = 0$ such that

$$|\mathbf{r}_s| \approx |\mathbf{r}_s|_{t=0} + \left(\frac{d}{dt}|\mathbf{r}_s|_{t=0}\right)t \quad \approx (r_{c0} + s_r) + \left(\frac{d}{dt}|\mathbf{r}_c|_{t=0} - \left(\frac{v_x}{r_{c0}}\right)s_x\right)t. \tag{9}$$

From this we observe that the range-offset s_r is manifest in the constant term, and the cross-range offset s_x is manifest in the linear (range-rate) term. Of course, a range-rate imparts a Doppler shift to a radar echo that also manifests as a pulse-to-pulse phase shift. Consequently, cross-range offset is associated with Doppler frequency.

The radar measures $|\mathbf{r}_s|$ and estimates retro-reflector location coordinates as

$$\hat{s}_r \approx |\mathbf{r}_s|_{t=0} - r_{c0}, \text{ and}$$
$$\hat{s}_x = -\frac{r_{c0}}{v_x}\left(\frac{d}{dt}|\mathbf{r}_s|_{t=0} - \frac{d}{dt}|\mathbf{r}_c|_{t=0}\right). \tag{10}$$

Note that

$$\frac{d}{dt}|\mathbf{r}_s| = \text{result of a radar measurement, and}$$
$$\frac{d}{dt}|\mathbf{r}_c| = \text{result of a navigator output.} \tag{11}$$

We stress that Eq. (10) assumes perfect navigator positions and velocity.

2.2 Red Pill

We now add errors to the navigator output that are unknown to the radar processor. This is illustrated in Figure 3.

Relative to a fixed-earth coordinate frame, we clarify and define the following points.

APC = Presumed Antenna Phase Center, i.e. where the radar thinks it is,
APC' = Actual Antenna Phase Center, i.e. where the radar really is,
SRP = Presumed Scene Reference Point, and
SRP' = Effective Scene Reference Point. (12)

We now define the APC position error, stipulated to be possibly time-varying, as

$\boldsymbol{\varepsilon}_{APC}$ = the relative location from the APC to APC', and
$\boldsymbol{\varepsilon}_{SRP}$ = the relative location from the SRP to SRP'. (13)

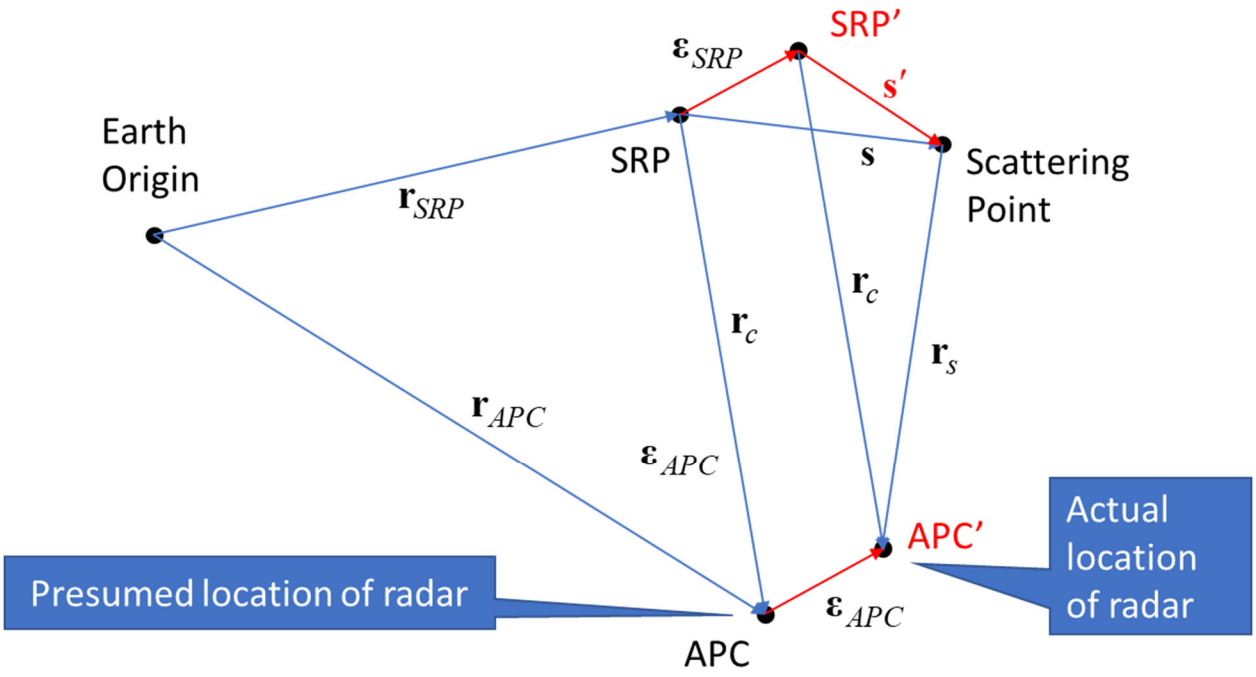

Figure 3. Geometry of SAR data collection with navigator errors.

We note that these are equal, that is

$$\boldsymbol{\varepsilon}_{SRP} = \boldsymbol{\varepsilon}_{ACP} . \tag{14}$$

In any case, these errors are unknown to the radar.

Relevant vectors are

$\mathbf{r}_c = \mathbf{r}_{APC} - \mathbf{r}_{SRP}$ = relative location of APC from SRP, as before
$\mathbf{s}' = \mathbf{s} - \boldsymbol{\varepsilon}_{SRP}$ = relative location of scattering point from SRP', and
$\mathbf{r}_s = \mathbf{r}_c - \mathbf{s}'$ = relative location of APC' from scattering point location. (15)

Of these,

$\mathbf{r}_{APC}$ is measured by the radar's navigator, as before, but has errors,
$\mathbf{r}_{SRP}$ is specified as an input to calculations,
$\mathbf{r}_c$ is calculated from navigation measurement data, but now contains errors,
$|\mathbf{r}_s|$ is measured by radar echo soundings, as before, and
$\mathbf{s}'$ is calculated from a comparison of radar measurements to navigator calculations. (16)

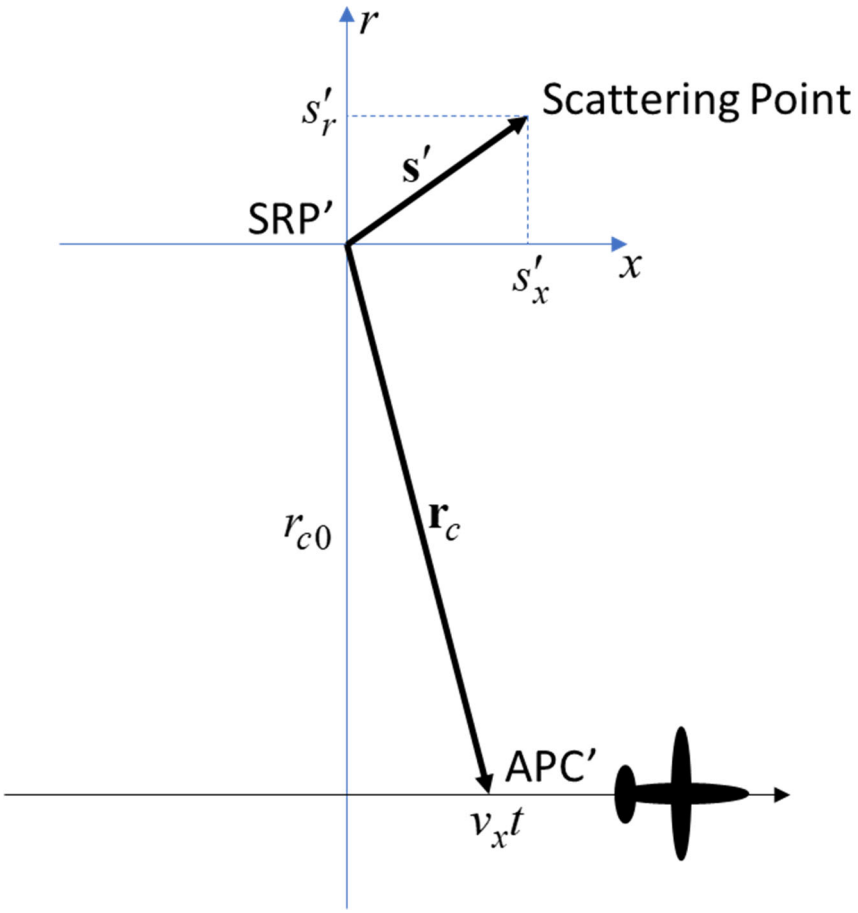

Figure 4. 2-D model with navigator errors and with coordinate frame defined.

At a high level, but sufficient for our purposes, we will now assume the 2-D model in Figure 2 becomes the 2-D model in Figure 4, where we have essentially replaced SRP and APC with SRP' and APC' respectively. Accordingly, we define

$$\begin{aligned}
&\left(s'_x, s'_r\right) = \text{coordinates for the scattering point location, assumed to be constants for SAR,} \\
&\left(\varepsilon_x, \varepsilon_r\right) = \text{coordinate offsets of navigator error, possibly time-varying, and} \\
&\left(v_x t\,, -r_{c0}\right) = \text{coordinates for the APC, which moves with time,}
\end{aligned} \tag{17}$$

where

$$\begin{aligned}
&v_x = \text{cross-range velocity,} \\
&t = \text{time referenced to the center of the actual synthetic aperture, and} \\
&r_{c0} = \text{the scalar range from SRP' to the APC' at time } t = 0\,.
\end{aligned} \tag{18}$$

With these definitions, we identify

$$\left|\mathbf{r}_s\right| = \sqrt{\left(\mathbf{r}_c + \boldsymbol{\varepsilon}_{APC} - \mathbf{s}\right) \bullet \left(\mathbf{r}_c + \boldsymbol{\varepsilon}_{APC} - \mathbf{s}\right)}, \tag{19}$$

which can be expanded to

$$\left|\mathbf{r}_s\right| = \sqrt{\left|\mathbf{r}_c\right|^2 + \left|\boldsymbol{\varepsilon}_{APC}\right|^2 + \left|\mathbf{s}\right|^2 + 2\mathbf{r}_c \bullet \boldsymbol{\varepsilon}_{APC} - 2\mathbf{r}_c \bullet \mathbf{s} - 2\mathbf{r}_c \bullet \boldsymbol{\varepsilon}_{APC}}\,. \tag{20}$$

We now identify coordinates for the various entities as

$$\begin{aligned} &\mathbf{r}_c \rightarrow \left(v_x t\,, -r_{c0}\right), \\ &\mathbf{s} \rightarrow \left(s_x\,, s_r\right), \text{ and} \\ &\boldsymbol{\varepsilon}_{APC} \rightarrow \left(\varepsilon_x\,, \varepsilon_r\right). \end{aligned} \tag{21}$$

Furthermore, we allow linear rates of change in both error components such that

$$\begin{aligned} &\varepsilon_r = \varepsilon_{r0} + \varepsilon_{r1}\, t\,, \text{ and} \\ &\varepsilon_x = \varepsilon_{x0} + \varepsilon_{x1}\, t\,. \end{aligned} \tag{22}$$

We linearize Eq. (20) to

$$\left|\mathbf{r}_s\right| \approx \left|\mathbf{r}_s\right|_{t=0} + \left(\frac{d}{dt}\left|\mathbf{r}_s\right|_{t=0}\right) t\,. \tag{23}$$

Specifically, component terms of Eq. (23) are calculated to be

$$\begin{aligned} &\left|\mathbf{r}_s\right|_{t=0} \approx r_{c0} + s_r - \varepsilon_{r0}\,, \text{ and} \\ &\frac{d}{dt}\left|\mathbf{r}_s\right|_{t=0} \approx \frac{d}{dt}\left|\mathbf{r}_c\right|_{t=0} - \frac{\left(s_x - \varepsilon_{x0}\right)}{r_{c0}}\left(v_x + \varepsilon_{x1}\right) - \varepsilon_{r1}\,. \end{aligned} \tag{24}$$

From this we observe that the range-offset s_r is manifest in the constant term, and the cross-range offset s_x is manifest in the linear (range-rate) term.

However, the radar being unaware of any errors, measures $\left|\mathbf{r}_s\right|$ and estimates scattering point location coordinates still as given in Eq. (10), repeated here as

$$\begin{aligned} &\hat{s}_r \approx \left|\mathbf{r}_s\right|_{t=0} - r_{c0}, \text{ and} \\ &\hat{s}_x = -\frac{r_{c0}}{v_x}\left(\frac{d}{dt}\left|\mathbf{r}_s\right|_{t=0} - \frac{d}{dt}\left|\mathbf{r}_c\right|_{t=0}\right). \end{aligned} \tag{25}$$

Note that it remains that

$$\frac{d}{dt}\left|\mathbf{r}_s\right| = \text{result of a radar measurement, and}$$
$$\frac{d}{dt}\left|\mathbf{r}_c\right| = \text{result of a navigator output.} \tag{26}$$

Solving for scattering point location coordinates, and relating them to the reported values in Eq. (25) yields the true scattering point location coordinates in terms of the estimated values as

$$s_r \approx \hat{s}_r + \varepsilon_{r0}, \text{ and}$$
$$s_x = \hat{s}_x\left(1+\frac{\varepsilon_{x1}}{v_x}\right)^{-1} + \varepsilon_{x0} - \frac{r_{c0}}{v_x}\varepsilon_{r1}\left(1+\frac{\varepsilon_{x1}}{v_x}\right)^{-1}. \tag{27}$$

We offer the following observations and comments.

- The navigator error $\boldsymbol{\varepsilon}_{APC}$ directly generates an equivalent geolocation error in a SAR image scattering point location.
- The factor ε_{r1} is the linear rate of change in the range position error; a line-of-sight range-rate (velocity) error.
- In addition, a linear rate of change in the ε_r error component will generate an additional error in the SAR cross-range location of an image scattering point.
- The factor ε_{x1} is the linear rate of change in the cross-range position error; a cross-range range-rate (velocity) error.
- A linear rate of change in the error in the ε_x error component will affect the SAR cross-range scattering point location error by scaling the cross-range offset of the scattering point location.
- A reasonable expectation might then be that the cross-range geolocation error is statistically worse than the line-of-sight range geolocation error.

3 Navigator Accuracy

We examine in this section the typical performance of a navigator with architecture of a GPS-aided IMU. These are common for SAR systems, and are exemplified in a paper by Kim, et al.[2]

We will find it useful to have an idea of timescale over which we need motion statistics; the interval over which we need to understand the motion measurement errors. We declare this to be the time-interval of a synthetic aperture, which we calculate as

$$T_a = \frac{a_{wa}\lambda r_{c0}}{2\rho_a v_x} \text{ = synthetic aperture time,} \tag{28}$$

where we introduce the parameters

a_{wa} = cross-range Impulse-Response (IPR) broadening factor, due to data tapering,
λ = nominal wavelength of the radar signal, and
ρ_a = nominal cross-range resolution of the radar. (29)

Example

We note that for a Ku-band SAR, with parameters

a_{wa} = 1.2,
λ = 0.018 m,
r_{c0} = 100 km,
ρ_a = 0.3 m, and
v_x = 50 m/s, (30)

the synthetic aperture time calculates to 72 seconds.

3.1 GPS

GPS performance with respect to accuracy and precision is studied and reported in a number of publications. In particular, we will draw information from two reports; a report of analysis performed for the Federal Aviation Administration (FAA),[3] and a report by the University of Texas at Austin (UT-Austin) for the US Navy.[4] These reports deal with the L1 C/A code mode of operation. We forgo any discussion of more advanced modes that use additional bands, P(Y) codes, differential operation, etc. Furthermore, we discuss only the "capabilities" of GPS, irrespective of any non-ideal GPS receiver limitations. We are mindful that a GPS receiver can always be built such as to degrade performance from that which it might otherwise be capable.

Like any system, GPS was designed and built to provide some degree of guaranteed performance. But also like any well-designed system, the typical performance is much better than the guaranteed performance.

From the FAA report, the GPS requirement is to provide a "Global Average Position Domain Accuracy" better than 9 m horizontal error 95% of the time. However, the measured horizontal position error averaged over 28 Wide Area Augmentation System (WAAS) reference station sites was better than 1.9 m 95% of the time over the 3-month period 1 October to 31 December 2016. The histogram data from which these statistics were calculated has the appearance of a very "Rayleigh-like" horizontal error distribution. This suggests a Rayleigh scale-factor of 0.77 m, which also suggests an underlying overall zero-mean 2-D Gaussian distribution with an RMS error of 0.77 m for the marginal distribution in any particular orientation, such as in dimensions of radar range and cross-range. The UT-Austin report gave comparable results.

Anecdotal measurements confirm RMS errors on the order of a meter or less in each of orthogonal horizontal directions.‡ In addition, the position measurements are somewhat noisy from one second to the next, on top of a slowly varying drift.

This also begs the question "How persistent/stable is the error?" That is, we require knowledge of how fast the error changes with time so that we might gauge the timescale of its fluctuations. While the cited reports don't explicitly calculate this, they do provide information that allows us to infer some limits. The FAA report provides range-rate error statistics and range-acceleration error statistics for each of the 32 GPS satellites over the monitoring period. The range-rate error tended to be no greater than 2.5 to 3.0 mm/s 95% of the time, and the range-acceleration error tended to be no greater than 20 to 25 $\mu m/s^2$ 95% of the time. In both cases, maximum values were quite a bit larger, but just rare.

While we might reasonably expect the net horizontal position-drift due to processing multiple satellites' data to be less than the range-rate values for any individual satellite, even equating the horizontal position-drift to 3.0 mm/s sustained for the 72 seconds of our example would yield only a 0.22 m change in the horizontal position error. This is substantially less than the 0.77 m RMS error previously calculated. We also note that a sustained range-acceleration error value of

‡ See Appendix B.

25 μm/s^2 yields a range-rate error change of 1.8 mm/s over 72 seconds, suggesting that we have no reason to suspect wild range-rate swings during the synthetic aperture, at least most of the time.

The aforementioned anecdotal evidence further indicates a high degree of correlation for adjacent samples that falls off with time separation or difference.‡ We are particularly interested in intervals that represent realistic synthetic aperture length, say 10 seconds to perhaps 200 seconds. Specifically, for this span of intervals,

- The RMS standard deviation grows approximately logarithmically with observational interval length between 10 and 1000 seconds, with an RMS standard deviation of about 15 cm over a 200-second interval, with only about 9 cm over the 72-second interval of our example, in each of orthogonal horizontal directions.

- The RMS drift rate falls off approximately logarithmically with observational interval length between 10 and 400 seconds, with an RMS rate of about 2.3 mm/s over a 200 second interval, with an RMS rate of about 4.3 mm/s over the 72-second interval of our example.

- The drift rate, when sustained over the observation interval, yields an RMS position error that grows approximately logarithmically with observational interval length between 10 and 400 seconds, with an RMS displacement at the ends of the interval of about 22 cm for a 200-second interval, but only 16 cm for our 72-second example.

These measured statistics suggest that the error in range and in cross-range can be treated as essentially a constant or bias within a synthetic aperture, but random (albeit highly correlated) from one synthetic aperture to the next with an overall 0.77 m RMS value, at least 95% of the time, for the example presented.

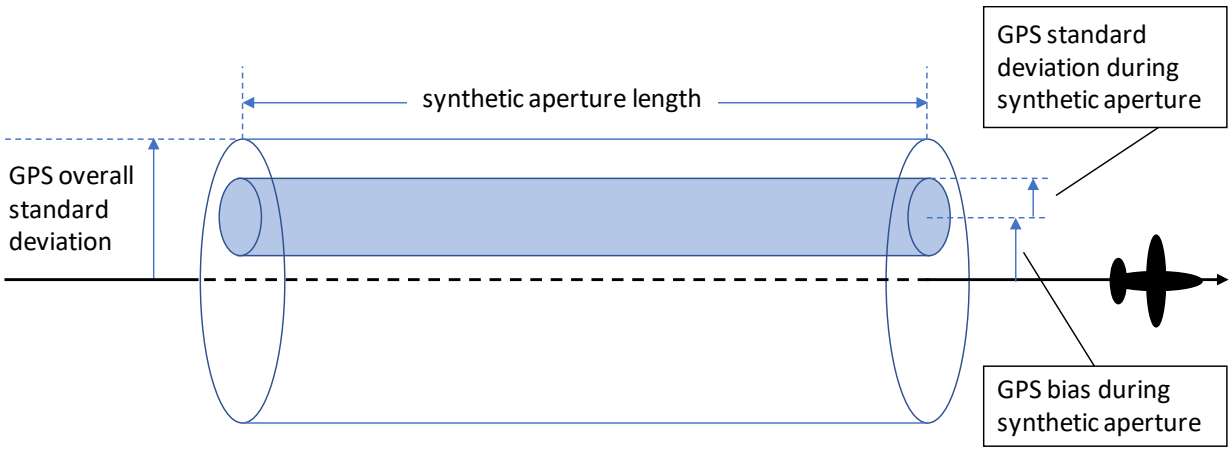

Figure 5. Notional error model for GPS errors. Over the observational interval of a synthetic aperture, the GPS position error manifests as a bias with some random variations around it. As the observation interval grows, the bias tends towards zero, and the interval's standard deviation approaches that of the overall GPS accuracy.

However, even as we treat the GPS position error as essentially a bias, we still need to allow for some degree of position drift during the synthetic aperture. To the extent that GPS range-rate contributes to horizontal position-drift, and hence to radar-range-error rate, we might bound the SAR geolocation range-error rate to the heuristic equation

$$v_{\varepsilon,RMS}(T_a) = 13.0 - 4.6\log_{10}(T_a) \quad \text{mm/s}, \quad \text{for } 10 \le T_a \le 400\,. \tag{31}$$

For radar motion measurement, it is not sufficient to know only "where" the radar is, but we also need to know "when" the radar was at that location. The FAA report also provides statistics on Time Transfer Error, noting that the error for all satellites during the monitoring period was no greater than 10 ns for 95% of the time. We note that during 10 ns, a radar travelling at 50 m/s will travel only 0.5 mm, inconsequential compared to other errors.

We briefly summarize relevant GPS attributes as follows.

Pros:

GPS provides overall bounds on position errors.

GPS provides even tighter bounds on position error drifting around some bias level during a synthetic aperture.

Cons:

GPS, with its relatively slow sample rate (e.g. updates on the order of a second) is not able to unambiguously measure motion frequencies higher than about 1/2 Hz or so.

As specific satellites become observable, and others drop out, sudden jumps of perhaps more than a radar wavelength in calculated (and reported) position might be observed during a synthetic aperture. SAR image formation that relies on this unfiltered motion measurement would be adversely affected, both in focusing and perhaps geolocation.

3.2 IMU

IMU performance as it relates to SAR imaging is discussed in some detail in an earlier report.[5]

The IMU instrument is typically comprised of three accelerometers arranged to measure accelerations in orthogonal directions, and three angular-rate sensors (rate-gyros) arranged to measure rotational rates around orthogonal axes.

Measured accelerations are integrated to provide velocity information, and these velocities are integrated again to provide position information. Measured angular rates are integrated to provide angular orientation. Any noise in raw accelerometer or rate-gyro data, when integrated, causes random errors in the velocities, positions, and orientation angles. Absent any correction, these errors can grow without bound.

Constraining this otherwise unbounded error growth is the purpose of aiding. Note that if the IMU were "perfect," that is without error, after an initial alignment the IMU would need no further aiding at all. However, a world with perfect IMUs is also one with unicorns and pigs that can fly. Nevertheless, some IMUs are closer to perfect than others, implying that the proper degree of aiding will depend on the underlying goodness of the IMU. For the following development, we borrow heavily from the aforementioned report. We refer the reader to the report for details.

From the aforementioned report, we understand that the relevant acceleration error due to accelerometers in a particular direction is described to be

$$a_\varepsilon = \begin{pmatrix} \beta a_t + \beta_a |a_t| + \beta_n a_t^{\,2} + a_\perp \sin(\phi_m + \phi_n) \\ +b_{a,0} + n_{a,q} + n_{a,0} + n_{a,1} + n_{a,2} \end{pmatrix} \tag{32}$$

where

a_t = true acceleration in the desired measurement direction,
β = scale factor error.
β_a = scale factor asymmetry,
β_n = scale factor nonlinearity,
$a_\perp$ = true acceleration in the orthogonal (perpendicular) direction,
φ_m = angular misalignment error,
φ_n = angular nonorthogonality error,
$b_{a,0}$ = constant bias error,
$n_{a,q}$ = quantization noise,
$n_{a,0}$ = white noise error (velocity random walk error source),
$n_{a,1}$ = flicker noise error, and
$n_{a,2}$ = acceleration random walk error. (33)

Also relevant are the angular rate errors, for which relevant parameters around a particular axis can be described by

$$\omega_\varepsilon = \omega_m - \omega_t = \begin{pmatrix} \gamma\omega_t + \gamma_a|\omega_t| + \gamma_n{\omega_t}^2 + \omega_\perp \sin(\phi_m + \phi_n) \\ + b_{\omega,0} + n_{\omega,q} + n_{\omega,0} + n_{\omega,1} + n_{\omega,2} \end{pmatrix} \tag{34}$$

where

ω_t = true angular rate in the desired measurement direction,
γ = scale factor error.
γ_a = scale factor asymmetry,
γ_n = scale factor nonlinearity,
$\omega_\perp$ = true angular rate in the orthogonal (perpendicular) direction,
ϕ_m = angular misalignment error,
ϕ_n = angular nonorthogonality error,
$b_{\omega,0}$ = constant bias error,
$n_{\omega,q}$ = quantization noise,
$n_{\omega,0}$ = white noise error (angular random walk error source),
$n_{\omega,1}$ = flicker noise error, and
$n_{\omega,2}$ = rate random walk error. (35)

Both instrument acceleration errors as well as angular rate errors will impact the final calculated position error. We will presume that scale factors, misalignments, and biases can be adequately mitigated by subsequent calibration and filtering. This leaves only the noise terms remaining to generate and influence a position error. Of these, the quantization noise is expected to be small compared to other sources. Of the remaining noise sources, Allan variance analysis shows that different components dominate on different timescales, but we will keep them for now.

We also comment that even for constant-speed, straight and level flight, the IMU is still subject to acceleration due to gravity. In fact, we might expect gravity to generally dominate accelerations for benign radar flight paths. Accordingly, we define

$g = 9.8$ m/s^2 = acceleration due to gravity. (36)

If we assume a perfectly aligned IMU at time $t = 0$, then at some later time t we may estimate the angular error relevant to projecting gravity in the range direction as

$$\theta_\varepsilon(t) = \left(\int_0^t n_{\omega,0} d\tau + \int_0^t n_{\omega,1} d\tau + \int_0^t n_{\omega,2} d\tau \right), \tag{37}$$

and the velocity error as the integrated errors due to accelerations, including gravity, as

$$v_\varepsilon(t) = \left(\int_0^t n_{a,0} d\tau + \int_0^t n_{a,1} d\tau + \int_0^t n_{a,2} d\tau + g \int_0^t \theta_\varepsilon(\tau) d\tau \right), \tag{38}$$

and the corresponding range error as simply the integrated velocity error, as

$$r_\varepsilon(t) = \int_0^t v_\varepsilon(\tau) d\tau \,. \tag{39}$$

Note how angular errors cause gravity to couple into range error.

The noise terms are all presumed to be uncorrelated with each other, and have individual Power Spectral Density (PSD) functions given by

$$\begin{aligned}
S_{N_\alpha}(f) &= N_\alpha^2 \quad (\mu g)^2 / Hz \text{ , for } n_{a,0} \,, \\
S_{B_\alpha}(f) &= \frac{B_\alpha^2}{2\pi |f|} \quad (\mu g)^2 / Hz \text{ , for } n_{a,1} \,, \\
S_{K_\alpha}(f) &= \frac{K_\alpha^2}{(2\pi f)^2} \quad (\mu g)^2 / Hz \text{ , for } n_{a,2} \,, \\
S_{N_\omega}(f) &= 3600 N_\omega^2 \quad (^\circ/h)^2 / Hz \text{ , for } n_{\omega,0} \,, \\
S_{B_\omega}(f) &= \frac{B_\omega^2}{2\pi |f|} \quad (^\circ/h)^2 / Hz \text{ , for } n_{\omega,1} \,, \\
S_{K_\omega}(f) &= \frac{K_\omega^2}{3600(2\pi f)^2} \quad (^\circ/h)^2 / Hz \text{ , for } n_{\omega,2} \,,
\end{aligned} \tag{40}$$

where the IMU-specific parameters are

N_α = white noise parameter responsible for acceleration random walk ($\mu g / \sqrt{Hz}$),
B_α = acceleration bias instability parameter (μg),
K_α = acceleration random walk parameter ($\mu g / s^{1/2}$),
N_ω = angular white noise parameter responsible for angular random walk ($^\circ / \sqrt{h}$),
B_ω = angular bias instability parameter ($^\circ / h$), and
K_ω = angular rate random walk parameter ($^\circ / h^{3/2}$). (41)

Subsequent analysis will need to be mindful of unit conversions. In addition, manufacturer data sheets do not always provide representative values for all of the IMU parameters in Eq. (41).

Expected total variance in the angle error, accounting for unit conversions, may be calculated to be

$$\sigma_{\theta_\varepsilon}^2 = \left(\frac{\pi/180}{3600}\right)^2 3600 N_\omega^2(t) + \left(\frac{\pi/180}{3600}\right)^2 B_\omega^2\left(\frac{t^2}{2}\right) + \left(\frac{\pi/180}{3600}\right)^2 \frac{K_\omega^2}{3600}\left(\frac{t^3}{3}\right). \tag{42}$$

Expected total variance in the velocity error, accounting for unit conversions, may be calculated to be

$$\sigma_{v_\varepsilon}^2 = (9.8)^2 \left(\begin{array}{l} \left(10^{-6}\right)^2 N_\alpha^2(t) + \left(10^{-6}\right)^2 B_\alpha^2\left(\frac{t^2}{2}\right) + \left(10^{-6}\right)^2 K_\alpha^2\left(\frac{t^3}{3}\right) \\ + \left(\frac{\pi/180}{3600}\right)^2 3600 N_\omega^2\left(\frac{t^3}{3}\right) + \left(\frac{\pi/180}{3600}\right)^2 B_\omega^2\left(\frac{t^4}{8}\right) + \left(\frac{\pi/180}{3600}\right)^2 \frac{K_\omega^2}{3600}\left(\frac{t^5}{20}\right) \end{array} \right). \tag{43}$$

Expected total variance in the range error, accounting for unit conversions, may be calculated to be

$$\sigma_{r_\varepsilon}^2 = (9.8)^2 \left(\begin{array}{l} \left(10^{-6}\right)^2 N_\alpha^2\left(\frac{t^3}{3}\right) + \left(10^{-6}\right)^2 B_\alpha^2\left(\frac{t^4}{8}\right) + \left(10^{-6}\right)^2 K_\alpha^2\left(\frac{t^5}{20}\right) \\ + \left(\frac{\pi/180}{3600}\right)^2 3600 N_\omega^2\left(\frac{t^5}{20}\right) + \left(\frac{\pi/180}{3600}\right)^2 B_\omega^2\left(\frac{t^6}{72}\right) + \left(\frac{\pi/180}{3600}\right)^2 \frac{K_\omega^2}{3600}\left(\frac{t^7}{252}\right) \end{array} \right). \tag{44}$$

In both cases, velocity and range, the error growth accelerates rapidly with time.

We illustrate IMU performance with the following example.

Example

Consider the following specifications for a popular tactical-grade IMU,

$$\begin{aligned} N_\alpha &= 16\ \mu g/\sqrt{Hz}\,, \\ B_\alpha &= 3.1\ \mu g\,, \\ K_\alpha &= \text{not given, presumed } 0\ \mu g/s^{1/2}\,, \\ N_\omega &= 0.07\ ^\circ/\sqrt{h}\,, \\ B_\omega &= 0.35\ ^\circ/h\,, \text{ and} \\ K_\omega &= \text{not given, presumed } 0\ ^\circ/h^{3/2}. \end{aligned} \tag{45}$$

If we presume a perfectly aligned IMU at time $t = 0$, then Figure 6 shows the growth of the expected RMS errors in angle, velocity, and position.

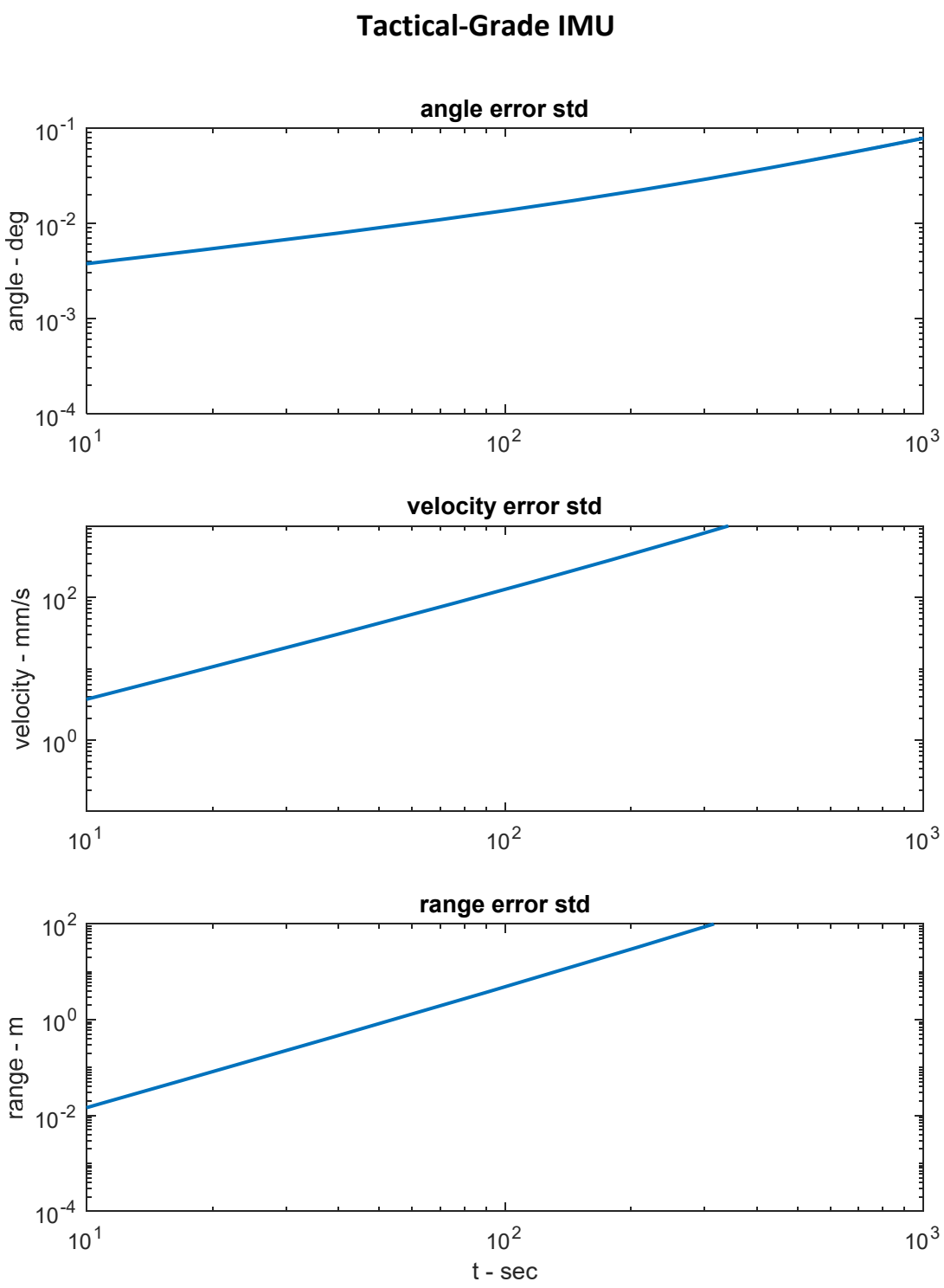

Figure 6. RMS error growth for a common tactical-grade IMU.

Our example illustrates the fairly common condition that gravity coupling due to angular errors are a principal source of velocity and range error.

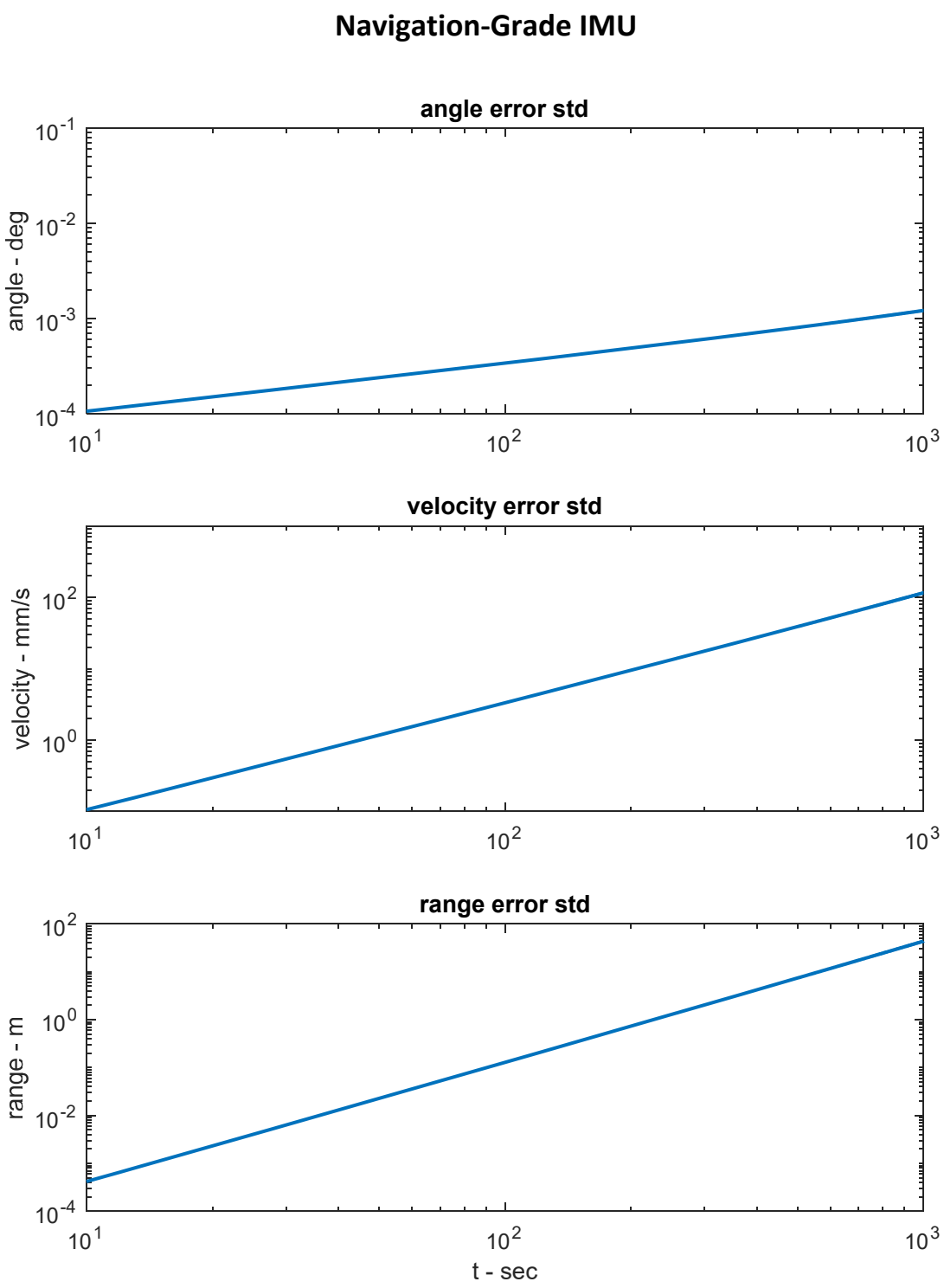

Figure 7. RMS error growth for a common navigation-grade IMU.

Example

Consider the following specifications for a popular navigation-grade IMU,

$$
\begin{aligned}
N_\alpha &= 0.6\ \mu g/\sqrt{Hz}\,, \\
B_\alpha &= \text{not given, presumed } 0\ \mu g\,, \\
K_\alpha &= \text{not given, presumed } 0\ \mu g/s^{1/2}\,, \\
N_\omega &= 0.002\ ^\circ/\sqrt{h}\,, \\
B_\omega &= 0.003\ ^\circ/h\,, \text{ and} \\
K_\omega &= \text{not given, presumed } 0\ ^\circ/h^{3/2}\,.
\end{aligned}
\tag{46}
$$

If we presume a perfectly aligned IMU at time $t = 0$, then Figure 7 shows the growth of the expected RMS errors in angle, velocity, and position.

We briefly summarize relevant IMU attributes as follows.

Pros:

With sample rates in the hundreds of Hz or higher, IMUs can unambiguously measure motion spectra also into the hundreds of Hz or so.

Cons:

Practical performance limits of IMU instruments (e.g. noise, biases, etc.) will cause drifts in the calculated position and orientation of the instruments without bound. Some error sources can be filtered or compensated, but random noise generally cannot.

3.3 GPS-Aided IMU Navigator

For SAR navigators, GPS and IMU data are normally combined so as to take advantage of their respective strengths and mitigate their respective weaknesses. We might expect that improvements in either GPS performance alone, or improvements in IMU performance alone, would improve the overall navigator performance, as would certainly improvements in both.

Combining GPS and IMU data is customarily done via a Kalman Filter (KF), or its enhanced version, the Extended Kalman Filter (EKF). Several strategies exist for doing so. Two popular strategies are

1. Use GPS to calibrate the IMU at the beginning of a synthetic aperture, and then not again until the synthetic aperture is completed. For the duration of the synthetic aperture, radar motion is derived from the IMU alone. GPS position jumps during a synthetic aperture are thus irrelevant.

2. Allow GPS to continuously update the IMU data, including during the synthetic aperture, via somewhat loosely coupling them in a manner to avoid the problematic jumps when satellites come and go. For example, navigator output errors when compared to GPS can be fed back into the navigator as acceleration biases to gently tug the navigator into alignment compared to the GPS.

There are no doubt other schemes, too. Of the options presented, we note that the first one probably requires a higher-quality IMU for the longer synthetic aperture lengths we are considering.

A secondary question is "Just how exactly do we want the navigator to match or use the GPS measurements?" Two main methods are employed.

1. We wish the velocity calculations of the navigator to match velocity derived from GPS measurements. This is sometimes termed "velocity-aiding."

2. We wish the position calculations of the navigator to match the GPS position measurements. This is sometimes termed "position-aiding."

Each has its proponents, although we opine that for SAR, and especially for geolocation applications, position error is a more important metric than velocity error.

In any case, it is the navigator output, after GPS and IMU have been combined, that is of concern to the SAR. It is essential for quality SAR image formation that any residual motion measurement errors be smooth, with no sudden jumps in position. This is because sudden jumps in position errors represent high-frequency motion errors that are not able to be mitigated by customary autofocus processing algorithms. The result is poor image quality.

For geolocation accuracy, we are mainly concerned with

1. Range and cross-range biases in the position error,
2. Position drift-rate in the range direction, and
3. Position drift-rate in the cross-range direction (to a much lesser extent).

While myriad variations and "tuning" of integration algorithms for GPS and IMU data exist, we will make the following general assumptions.

- Geolocation range and cross-range biases in the position error are dominated by GPS position accuracy. Recall that RMS position errors tend to be on the order of a meter or less.
- The impact of position drift-rate in the cross-range direction is relatively minor compared to other sources.
- The impact of position drift-rate in the range direction is significant, and more complicated to assess than the other error sources. At longer ranges, this error source typically dominates the others.

Given these observations, we will adopt the following geolocation error models

$$\begin{aligned} \varepsilon_{s_r} &= \left(\hat{s}_r - s_r\right) = -\varepsilon_{r0}, \text{ and} \\ \varepsilon_{s_x} &= \left(\hat{s}_x - s_x\right) \approx -\varepsilon_{x0} + \frac{r_{c0}}{v_x}\varepsilon_{r1}. \end{aligned} \tag{47}$$

The RMS error for these geolocation coordinates are

$$\begin{aligned} \sigma_{s_r} &= \sigma_{r0}, \text{ and} \\ \sigma_{s_x} &\approx \sqrt{\sigma_{x0}^2 + \left(\frac{r_{c0}}{v_x}\right)^2 \sigma_{r1}^2}, \end{aligned} \tag{48}$$

where we have assumed independent error components, with

$$\begin{aligned} \sigma_{r0} &= \text{standard deviation of } \varepsilon_{r0}, \\ \sigma_{x0} &= \text{standard deviation of } \varepsilon_{x0}, \text{ and} \\ \sigma_{r1} &= \text{standard deviation of } \varepsilon_{r1}. \end{aligned} \tag{49}$$

Navigator Range-Rate Error

As it is often the principal source of azimuth geolocation error, especially at long ranges, we examine the range-rate error in somewhat more detail here. We note that the range-rate error has the effect of tilting the synthetic aperture, as is illustrated in Figure 8. More generally, SAR geolocation depends on the position and orientation of the synthetic aperture.

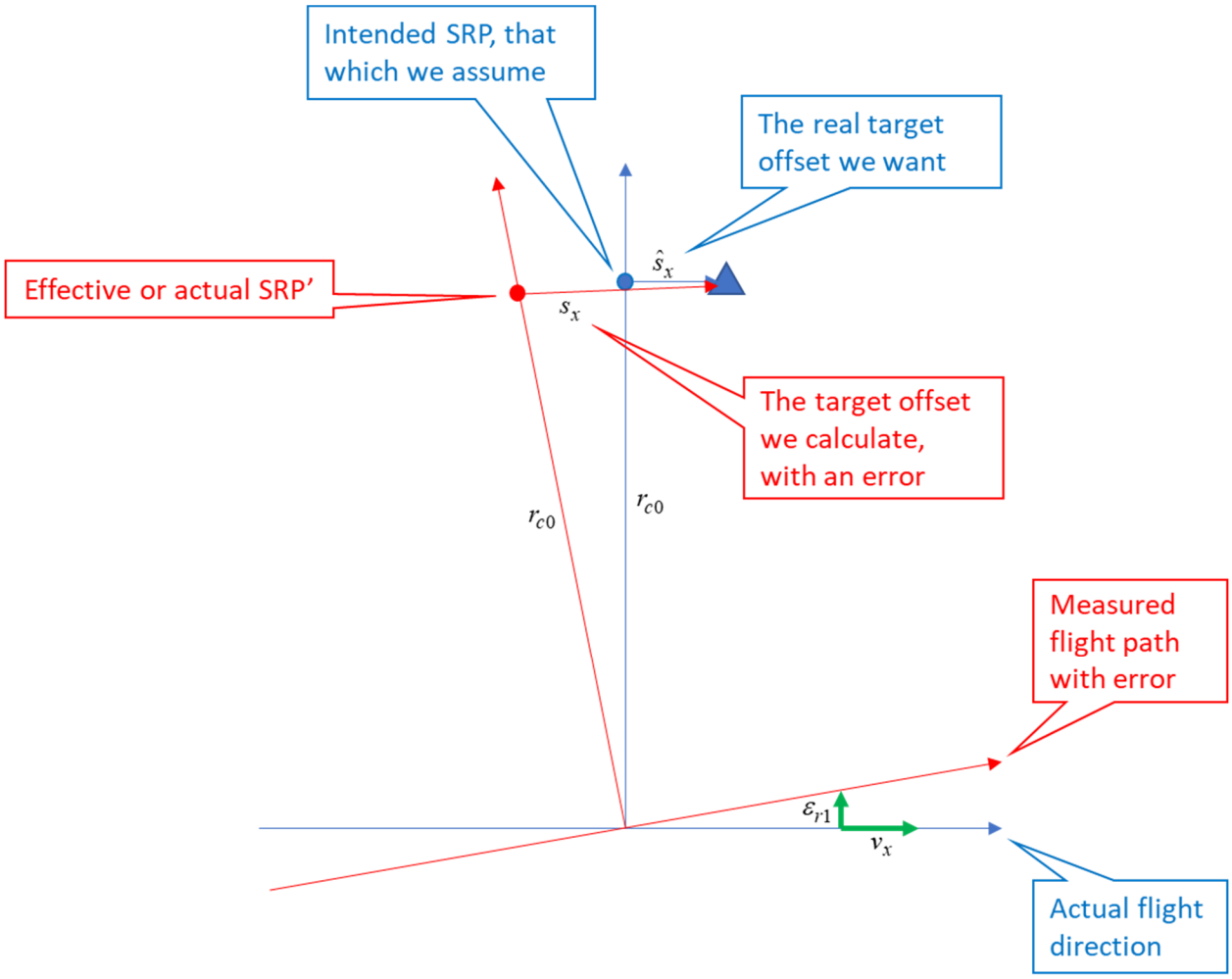

Figure 8. The range-rate error has the effect of tilting the synthetic aperture. This figure illustrates a broadside imaging geometry.

Note that both GPS as well as the integrated IMU data will exhibit errors in their assessment of the radar's range-rate towards the SRP. As their data are combined in the SAR navigator, we would expect the navigator output to also exhibit a range-rate error that depends on the blended values of GPS and IMU data in some fashion. The specific dependencies would of course depend on the details of how the GPS and IMU are blended.

In general, we might say that for very long synthetic apertures, owing to GPS's bounding of position errors, that the GPS solution expected net error drift rate would be superior to expected

velocity errors derived from an IMU alone, and hence should receive the greater weighting in a navigator. However, for very short synthetic apertures, the IMU's performance vis-à-vis residual velocity errors is probably better than what GPS might provide alone, and should receive the greater weighting in a navigator.

Consequently, it would seem that a navigator should blend GPS and IMU data so as to favor IMU-derived velocity information for short synthetic apertures, and GPS-derived velocity information for longer synthetic apertures. The question remains on how exactly to blend them and where a cross-over point might be as to which dominates in importance.

We will choose to presume that the navigator output is essentially the IMU-derived information, but continuously corrected to track GPS-derived measurements. Consequently, the net navigator range-rate will be a corrected IMU range-rate that "chases" the GPS range-rate, and likewise for the range-rate errors. There remain many details on time constants, convergence times, etc.

In anticipation of the following discussion, we offer a plot of synthetic aperture times as a function of range for various velocities in Figure 9. This is for 0.3-m cross-range (azimuth) resolution at Ku-band with a broadside imaging geometry. Note that synthetic aperture times do not appreciably exceed 100 seconds for 50 m/s radar velocity out to 150 km range.

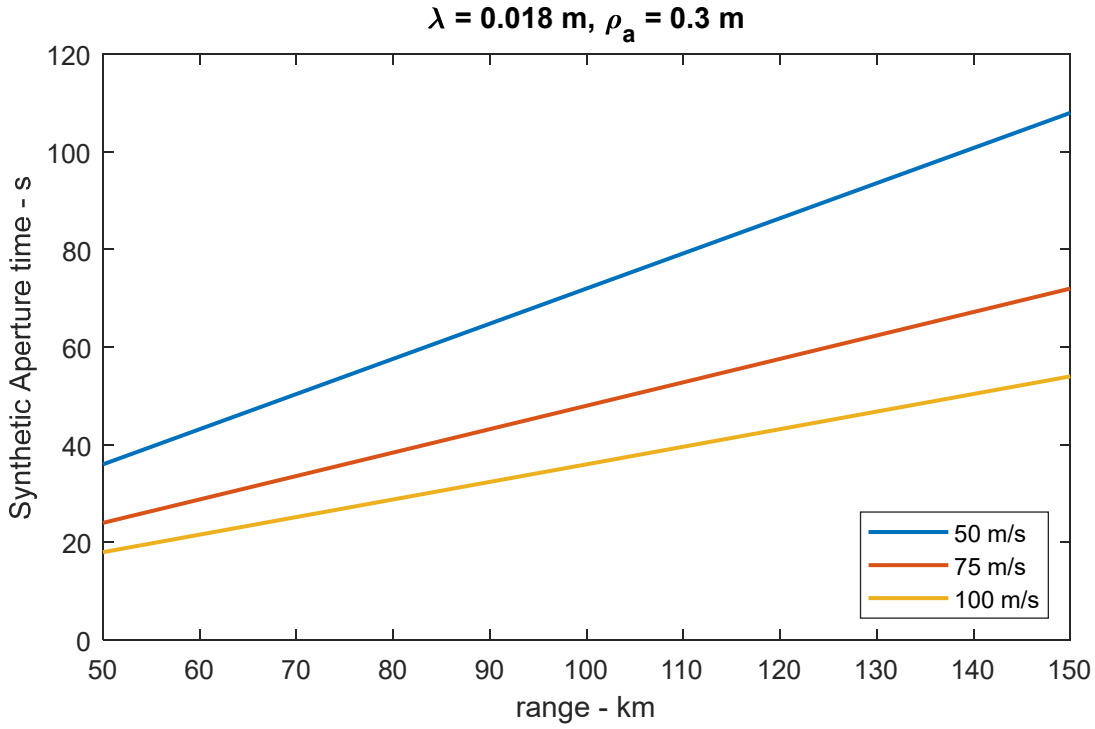

Figure 9. Synthetic aperture times for various radar velocities. Other parameters are as in Eq. (30).

Case 1: GPS-Limited

We assume here that the navigator range-rate error is essentially that of GPS, not otherwise significantly moderated by the IMU. Such would be the case when the convergence time of the navigator to the GPS solution is substantially less than the synthetic aperture length.

We may calculate the range-rate component of the expected RMS cross-range geolocation error as a function of range and velocity by combining Eq. (47) with the GPS behavior of Eq. (31) and Eq. (28) to yield the plot in Figure 10. Here we see cross-range geolocation error gets worse for longer ranges, and slower radar velocities, owing to longer-duration synthetic aperture times. Figure 11 illustrates RMS cross-range geolocation error for a finer 0.1-m azimuth resolution. Note the improved cross-range geolocation error. This is because the "tube" in Figure 5 is longer in spatial-length, allowing a net smaller linear range-rate component.

While geolocation accuracy depends on SAR azimuth resolution, it does not depend on range resolution. However, range-performance for SAR (defined in SNR terms) depends on range resolution, but not on azimuth resolution.[6] If we decouple range and azimuth resolution by allowing an image with finer azimuth resolution than range resolution, then we expect to get the same range performance (defined in SNR terms) but with improved geolocation error. A cost is a longer synthetic aperture time, and corresponding more complex image formation.

Case 2: Both GPS and IMU-Limited

We digress for the moment to considering a "perfect" IMU; one with no noise, biases, or other performance limitations or degradations. Such an IMU, once perfectly aligned, would yield perfect position and velocity measurements. It would require no additional GPS updates for the navigator to remain perfectly aligned.

Now consider just a "pretty-good" IMU, and contrast it with a "just-OK" IMU. A navigator with a pretty-good IMU probably doesn't need to chase GPS measurements to the same degree as a navigator with a just-OK IMU. We infer from this that a navigator can probably rely more, and for a longer period, on pretty-good IMU measurements, and converge slower to the GPS measurements, than doing so with a just-OK IMU. Inevitably, however, for a long enough synthetic aperture, the GPS bounds will ultimately assert themselves regardless of the IMU.

Now consider a navigator with the navigation-grade IMU of Figure 7. If perfectly aligned at time $t = 0$, then after 100 seconds without additional aiding will exhibit about a 3 mm/s RMS velocity error. Now let us consider a navigator with the same navigation-grade IMU, but with continuous aiding from GPS. We further presume that as a result of the aiding process, that the navigator output will limit range-rate errors to the lesser of the GPS range-rate error, or the 3 mm/s RMS derived from the IMU range-rate error. This of course all depends on how the navigator is tuned with respect to employing GPS versus IMU measurements. Nevertheless, with the presumption that range-rate error is bounded to 3 mm/s, Figure 12 shows expected RMS cross-range geolocation error as a function of range and velocity for 0.3-m azimuth resolution, and Figure 13 shows expected RMS cross-range geolocation error as a function of range and velocity for 0.1-m azimuth resolution.

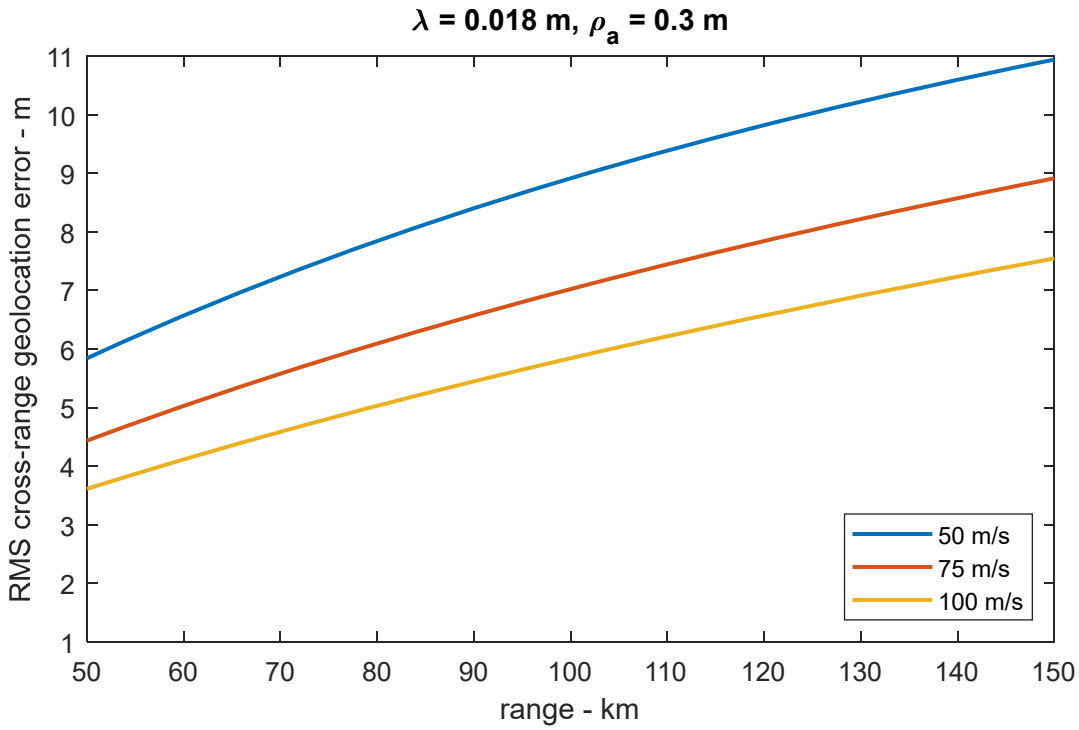

Figure 10. RMS cross-range geolocation error due to GPS range-rate error alone for various radar velocities.

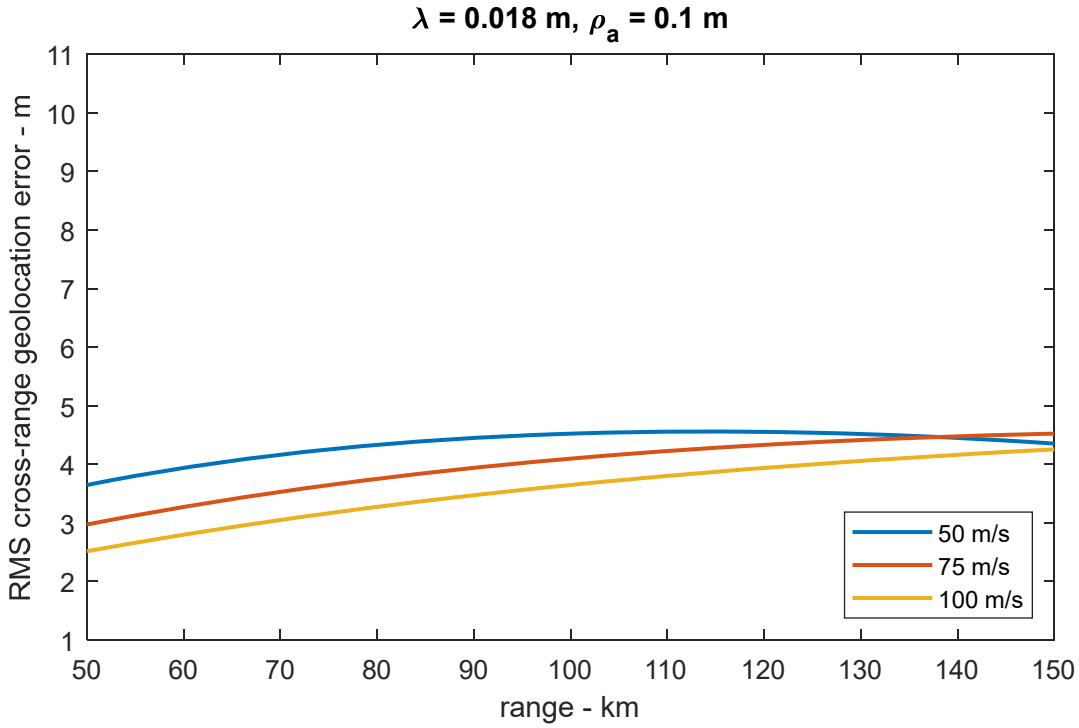

Figure 11. RMS cross-range geolocation error due to GPS range-rate error alone for various radar velocities.

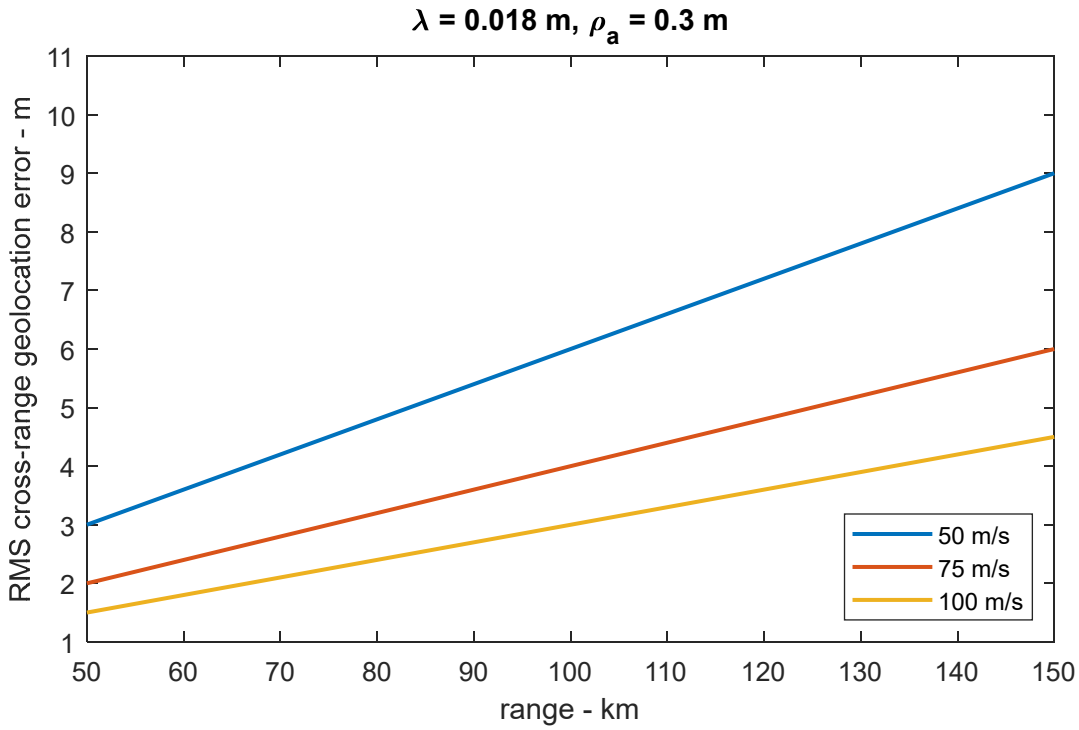

Figure 12. RMS cross-range geolocation error due to GPS range-rate error limited by 3 mm/s IMU velocity error for various radar velocities.

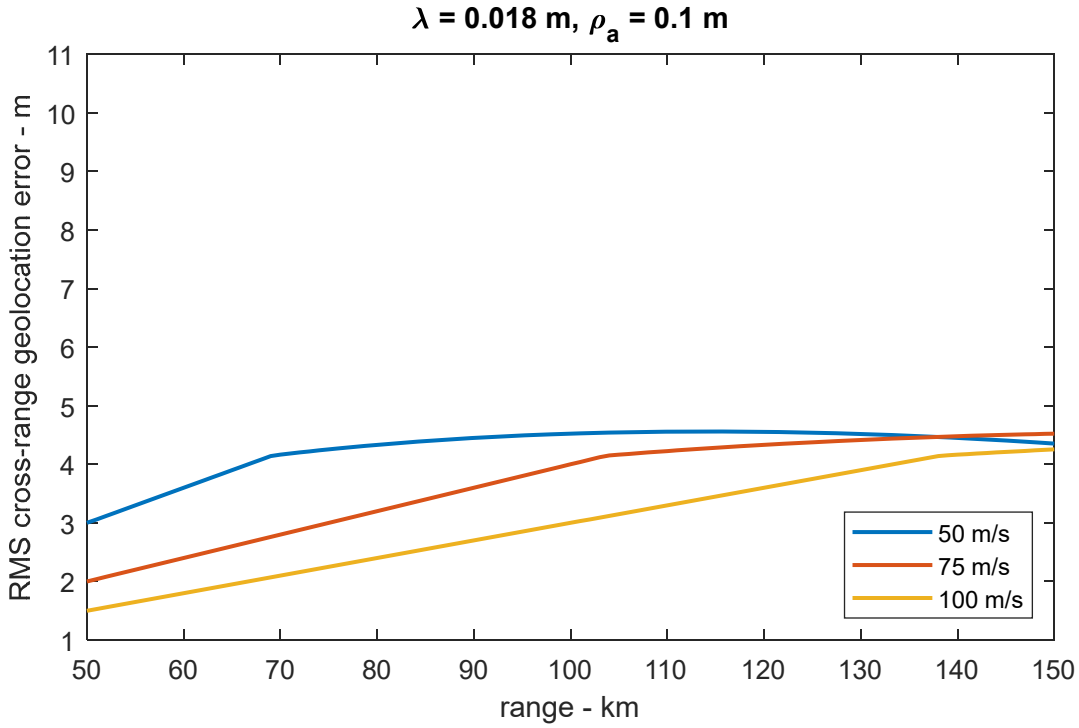

Figure 13. RMS cross-range geolocation error due to GPS range-rate error limited by 3 mm/s IMU velocity error for various radar velocities.

3.4 Comments

What follows are several related comments, and other points we wish to emphasize.

- SAR geolocation errors directly reflect navigator position error. However, a navigator range-rate error will strongly impact SAR cross-range geolocation error. At long ranges, this navigator range-rate will even be dominant to other sources.

- Over the timeframes of interest (synthetic aperture lengths) GPS errors manifest as a bias with random noise, but also a position drift that includes a problematic linear drift rate. Overall GPS position errors are bounded.

- IMU-derived position errors, absent any aiding, will increase without bound. A strong component of this is due to gravity coupling through gyro attitude errors.

- Better GPS, as in Differential-GPS (DGPS), would increase accuracy and precision of the GPS solution with smaller biases, but would also more tightly bound the position drift rate. This should have a direct consequence of improving SAR geolocation error.

- A better IMU, as previously noted, would allow a navigator to converge slower to a GPS solution, providing more immunity to GPS noise and drifting, especially over shorter durations. Inevitably, however, for a long enough synthetic aperture, the GPS bounds will ultimately assert themselves regardless of the IMU.

- Other aiding sources, including position, velocity, and attitude, might also improve navigator performance. It would depend on the nature of the aiding source. For example, an external navigation-grade IMU might offer a navigator improved performance over an indigenous tactical-grade IMU, but ultimately still be limited to GPS error bounds. Aligning one navigator to another is often called a transfer alignment.

- SAR images provide excellent relative position information. Consequently, if a fiducial image feature can be identified with a known adequately precise geolocation coordinate, then a relative offset from it would also provide an improved geolocation for some SAR image location under test. An extension of this would be registering a SAR image with another image database, say even an optical image database, with surveyed features.[7] Indeed, radar navigation and geolocation predates World War II.[8] It certainly predates GPS.

  We emphasize that this relative-geolocation is for geolocating scattering points in a SAR image, and not for back-calculating the radar's position, which requires accounting for other errors and biases.

“Errors using inadequate data are much less than those using no data at all.”
-- Charles Babbage

4 Geolocation Accuracy – Other Factors

Heretofore we have tacitly assumed that the SAR geolocation error depends exclusively on the navigator's error, derived from GPS and IMU errors, without regard for any errors in measuring the relative range between radar and SAR image location under test. This is embodied in Eq. (27) and Eq. (47). While this assumption served the purpose of examining the navigator's impact on SAR geolocation error, there are indeed other factors that also contribute, sometimes substantially, especially to the range component of geolocation, but also to the cross-range component. We briefly discuss some of them here.

We divide these other geolocation factors into four main classes of errors.

4.1 Ranging Accuracy

We are given that a radar measures range. Well, not quite.

The radar really measures echo time-delay, and calculates range based on an assumed velocity of propagation. Well, not quite.

The radar really uses an internal clock source, with a presumed known frequency, and associates some number of presumed clock-cycle periods with time delay.

Clock Accuracy and Precision

We offer as example a very typical oscillator specification in Table 1.

Table 1. Notional Oscillator Stability/Tuning Specification.

Source	*Spec*	*Units*
Aging Stability	±1	ppm (per year)
Temperature Stability	±5	ppm (–40 C to +50 C)
Mechanical Tuning	±5	ppm
Electrical Tuning	±0.5	ppm (±5 VDC)

Note that these are stability factors that render a frequency offset that can be considered constant over an entire synthetic aperture, as opposed to a phase noise that yields random frequency variations within a synthetic aperture.

A reasonable conclusion might be that this oscillator will maintain better than 10 parts-per-million (ppm) accuracy over the life of the radar, over its environmental specification. This

translates to a 10-ppm limit for range errors, which may be expressed as 1 m of range error for every 100 km of range.

If 10 ppm range error is deemed inadequate, then two options exist,

1) Get a better oscillator, and/or

2) Measure and compensate for the oscillator error.

The idea behind a better oscillator is to maintain frequency accuracy. This might include periodic calibration to counteract the aging, and a more temperature-controlled environment to enhance temperature stability.

The other scheme is to measure and compensate for the oscillator error. Compensation is merely recognizing that clock periods are not the nice, clean numbers that you thought they were, but rather will be 'stretched' or 'compressed' based on the actual measured clock deviation from nominal. The actual measurement is the more difficult task. One option is to compare a measured number of clock cycles with some more accurate timing marks, say derived from GPS.

Propagation Velocity

It is often convenient to assume a velocity of propagation equal to that of free space, namely

$$c_0 = 299,792,458 \text{ m/s}. \tag{50}$$

However, the atmosphere is decidedly not free space, exhibiting generally stratified dielectric properties that depend on temperature, humidity, pressure, altitude, etc. Humidity profiles are a principal source of error. The dielectric properties manifest as refraction and diminishments in the velocity of propagation, and can be quite significant. The free-space assumption can lead to an error in range calculation of tens of meters at a 100 km range.[9] A very typical range error for medium altitude operation might be in the neighborhood of 300 ppm, with the error indicating a longer range than true.

Evidence suggests that much of the range error can be mitigated by using a better model for stratified atmospheric humidity and its effects on propagation velocity. Nevertheless, atmospheric propagation is likely to remain a principal range error source.

4.2 Calibration Errors

Calibration remains the ugly stepchild of radar design and operation; often just an afterthought that belies its importance; making the difference between poor radar performance and extraordinary radar performance.

We begin this discussion by recalling that the radar at least intends to measure range to some SAR image location. However, we now address the question "Range from what?" That is, with respect to the radar system as a whole, just where exactly is the spot that we consider the location of the radar? From Figure 1 we have labelled the radar location as the Antenna Phase Center

(APC). This implies that we need to determine the antenna phase center location with respect to the mechanical structure of the antenna itself.[10,11]

Of course, with the phase center of the antenna identified, then this also needs to be the point for which the navigator provides position and motion estimates. Since the GPS antenna and the IMU are likely located somewhere else, we need to make sure their motion estimates are both properly transmogrified to the APC. This necessitates proper identification and measurements of appropriate lever arms to allow registration of the APC with corresponding navigation measurements. After all, we want to know where the APC is, and not some other part of the mechanical structure of the radar antenna or host aircraft.

Assuming a monostatic architecture, then both the transmitted signal and the received signal will effectively pass through the APC. However, an initiated transmit signal at the radar exciter will take some time to arrive at the APC, passing through circuits and cables to get there. Similarly, a signal received at the APC will take some time to traverse the receiver circuitry and cables to arrive at appropriate processing and recording elements, including perhaps conversion to digital data. In both cases, these provide additional delays to the signal which must be accounted or compensated during radar operation, lest they be judged as additional external propagation delay and hence generate range errors. However, it is essential that accommodating these delays in the radar's timing and control account for delays to/from the APC itself, and not some intermediate location like an antenna feed structure.

4.3 Layover Effects

Even with perfect range measurements, a remaining geolocation error source stems from the well-known phenomenon of "layover," sometimes called "foreshortening."

Layover is an artifact of a SAR image being a 2-D rendering of a 3-D scene, with the rendering having dimensions of slant-range and cross-range, or similar. Recall that cross-range is related to Doppler frequency offsets in the echo data. From Figure 14 we identify that constant range defines a sphere, and constant Doppler, or range-rate, defines a cone. Their intersection is a circle centered on the flight path. The circle intersects a ground-plane (or any other image reference plane) in as many as two places, with the antenna beam selecting which intersection providing the SAR image data. However, any feature above or below the ground on the circle and still in the antenna beam will map to the ground intersection point in the SAR image. They lay over onto the same image pixel.

Consider for the moment a broadside imaging geometry. For SAR image echo locations above, but still near the ground plane, their echo energy will appear as if at a nearer range on the ground plane, with an offset

$$\Delta r \approx \frac{-h_a h_s}{r_{c0}}, \tag{51}$$

where

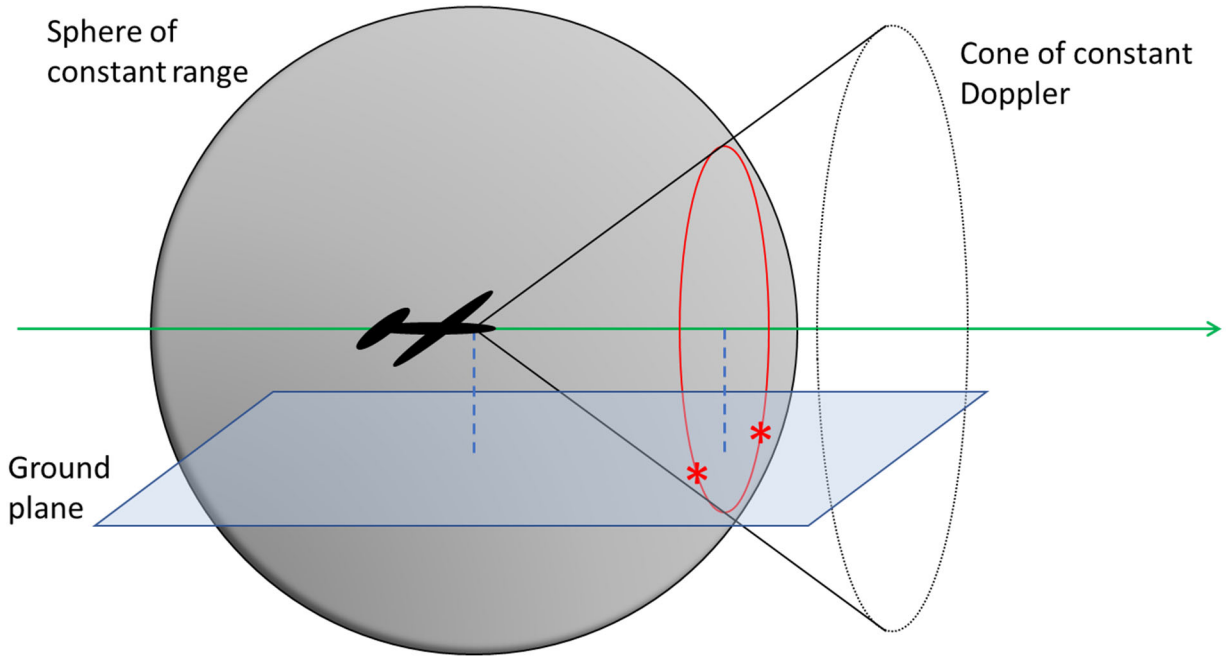

Figure 14. Graphical illustration of "layover." Constant range intersects constant Doppler on a circle, which intersects the ground-plane in at most two locations. The proper intersection is selected by the radar with its antenna beam.

h_a = height of the radar APC, and
h_s = height of the radar echo location above the ground plane. (52)

The negative sign indicates a height above the ground-plane leaning towards the radar.

Example

Consider a SAR broadside imaging geometry with parameters given as

r_{c0} = 50 km,
h_a = 20 kft = 6096 m, and
h_s = 10 m. (53)

The apparent range error is then calculated to be –1.22 m. Note that this is at about a 7-degree grazing angle. The error would be less at longer ranges, or lower APC heights; at shallower grazing angles.

Less appreciated, but no less true, is that at non-broadside imaging geometries the layover will be not only in range, but also in cross-range. This is readily apparent in Figure 14 where the "circle of layover" is not centered on the radar's APC. At these non-broadside squint angles, the range-layover remains as given in Eq. (51), but we now also manifest a cross-range-layover given by

$$\Delta a \approx \frac{-h_a h_s}{r_{c0}} \cot \theta_s , \tag{54}$$

where

θ_s = squint angle; the angle between flight path and radar echo location. (55)

Note that at broadside geometries, $\theta_s = \pm 90^\circ$, and the cross-range component of layover goes to zero. Since SAR images are rarely formed with squint angles more than 45 degrees from broadside, then the additional cross-range error due to layover will rarely be greater than the range-layover component. This component too will be less at longer ranges, or lower APC heights; at shallower grazing angles. In any case, to compensate for layover requires some means of estimating a pixel's elevation above/below the SRP.

There are techniques where the radar itself can determine a pixel's elevation, relative or absolute, for either an individual pixel, or a neighborhood of pixels, or even the entire SAR image. These techniques offer a spectrum of accuracies and precision. An exhaustive study of these techniques is beyond the scope of this report, but we briefly list some of them here as

1. Interferometric SAR (InSAR, or IFSAR), [12,13]
2. Stereo SAR, to include trilateration techniques,[14,15] and
3. Referencing to a fiducial point in the SAR image.

Of course, an ancillary map of altitude/height information might also be employed, and in fact might even be the preferred technique, especially with a single SAR image. Such a map in digital data form is termed a Digital Elevation Model/Map (DEM). A DEM might be used to estimate ground-level altitude in the vicinity of the SAR image pixel to be geolocated. Ideally, the SRP used by the radar would take this into account, else geolocating a pixel location in the SAR image certainly should do so. These techniques are termed Single-Image Geopositioning (SIG) techniques, as opposed to the Multiple-Image Geopositioning (MIG) techniques listed above.

Over the years, several descriptions and specifications have come, and sometimes gone, that define various levels of horizontal and vertical accuracy and precision.

A relatively early, but popular specification was the Digital Terrain Elevation Data (DTED) specification,[12] for which elements are given in Table 2. This was superseded by High-Resolution Terrain Information (HRTE) data. As of this writing the National Geospatial-Intelligence Agency (NGA) has adopted a standard that defines High Resolution Elevation (HRE) data standards, [16] for which elements are given in Table 3.

Table 2. Digital Terrain Elevation Data (DTED) level definitions.

DEM designation	*Post Spacing (approx.)*	*Absolute Height Accuracy*
DTED 0	900 m	Not specified
DTED 1	100 m	30 m LE90
DTED 2	30 m	18 m LE90
DTED 3 (proposed)	10 m	10 m
DTED 4 (proposed)	3 m	5 m
DTED 5 (proposed)	1 m	5 m

Table 3. High Resolution Elevation (HRE) level definitions.

DEM designation	*Post Spacing (approx.)*	*Absolute Height Accuracy*
HRE80	8 m	8 m LE90
HRE40	4 m	4 m LE90
HRE20	2 m	2 m LE90
HRE10	1 m	1 m LE90
HRE05	0.5 m	0.5 m LE90
HRE02	0.25 m	0.25 m LE90
HRE01	0.125 m	0.12 m LE90

SRTM

In 2000, the US' Space Shuttle flew the Shuttle Radar Topography Mission (SRTM), which implemented an earth-orbiting IFSAR.[17] The objective of this project was to produce digital topographic data for 80% of the Earth's land surface (all land areas between 60º north and 56° south latitude) to approximately DTED 2 accuracy and precision. This data is available from the US Geological Service (USGS).[18]

4.4 Miscellany

What follows are a miscellany of potential geolocation error sources.

Atmospheric Boundary Layer

The atmosphere was briefly discussed in a previous section, presented as a stratified dielectric that affects propagation velocity, and hence a source of potential range error. While generally true on a large scale, on a somewhat smaller scale the atmosphere exhibits sometimes sharp gradients and boundaries that aren't necessarily horizontally homogeneous. In fact, compelling evidence exists that sharp dielectric gradients can be quite "bumpy," meaning horizontal components to refraction.[19]

An examination of these phenomena and their effects on SAR image geolocation accuracy is beyond the scope of this report.

SAR Image Focus

Forming SAR images from long synthetic apertures often requires some amount of autofocus. The intent is to perform a blind deconvolution of delay/phase errors resulting from real or apparent motion measurement errors across the set of pulses. In particular, the intent is to compensate for non-linear phase errors, and improve cross-range focusing.

We recognize that applying any sort of linear phase "correction" will have the effect of shifting the SAR image in cross-range. Typically the linear-phase component of an autofocus correction is removed prior to its application. Any residual linear-phase component will affect SAR image geolocation.

Pixel Selection

Geolocating a feature in a SAR image ultimately requires selecting a pixel or pixels that contain the feature of interest. We presume this can be done to within the resolution of the radar image. This of course depends on the image being well-focused. We further stipulate that we need to remain mindful of radar glint and scintillation issues that might impact geolocation as well.

Recall that glint is defined as fluctuations in the angular direction or Doppler of a feature's echo response, whereas scintillation is often associated with fluctuations in the amplitude response of a radar scattering feature over time. Both are typically due the complex interactions of multiple scattering centers on a radar feature of interest.[20]

“Bear left”

“Right, frog”

-- Exchange between Kermit the Frog and Fozzy Bear in the Muppet Movie, 1979.

5 Conclusions

We repeat some key points.

- SAR image geolocation error can be considered to be a result of separable components:
  1. Range error, and
  2. Azimuth error.

  Errors in these components are sensitive to mostly different root causes.

- Both are dependent of radar own-ship location errors, generally less than 1 m RMS for GPS measurements.

- Azimuth location error, especially at long ranges, is very dependent on range-rate error, also known as line-of-sight-velocity error. This tends to be bounded at long ranges by GPS accuracy and precision. As synthetic aperture length increases, the IMU has diminishing influence.

- Range location error, especially at long ranges, is very dependent on delay-measurement error and the error in associating echo-delay with range, a large constituent of which is an error in the presumed velocity of propagation in the atmosphere.

- Calibration, especially of range/delay, is crucial to high quality ranging measurements.

“I am turned into a sort of machine for observing facts and grinding out conclusions.”
-- Charles Darwin

Appendix A – Geolocation Metrics

Consider a random geolocation error in two dimensions. Consider also that the location error in each dimension is uncorrelated zero-mean Gaussian, with identical variance, described with Probability Density Function (PDF) as

$$f_{X,Y}(x,y) = \frac{1}{2\pi\sigma^2} e^{-\frac{1}{2}\left(\frac{x^2}{\sigma^2}+\frac{y^2}{\sigma^2}\right)}, \tag{A1}$$

where

$$\sigma^2 \text{ = variance in either dimension.} \tag{A2}$$

The magnitude of the error is calculated as

$$r = \sqrt{x^2 + y^2}, \tag{A3}$$

and is described with a Rayleigh PDF as

$$f_R(r) = \frac{r}{\sigma^2} e^{-\frac{1}{2}\left(\frac{r^2}{\sigma^2}\right)}, \; r \geq 0. \tag{A4}$$

For this distribution, σ is called the "scale factor."

The Cumulative Density Function (CDF) is defined as the probability that some value is not exceeded, that is

$$CDF(r_0) = P\{r \leq r_0\}. \tag{A5}$$

For the Rayleigh PDF of Eq. (A4), this becomes

$$CDF(r_0) = \int_0^{r_0} f_R(r)\,dr = 1 - e^{-\frac{1}{2}\left(\frac{r_0^2}{\sigma^2}\right)}. \tag{A6}$$

We now define the Circular Error of Probability (CEP) function as that radius r_0 for which the CDF is some specified value. This is often written as

$$CEPxx = r_0 \text{ such that } CDF(r_0) = \frac{xx}{100}. \tag{A7}$$

We may solve Eq. (A6) to calculate *CEPxx* directly as

$$CEPxx = \sigma\sqrt{-2\ln\left(1-\left(\frac{xx}{100}\right)\right)}. \tag{A8}$$

CEP numbers of interest tend to be larger than the standard deviation of the underlying data. For example, we may calculate

$$\begin{aligned} &CEP50 = 1.18\ \sigma, \\ &CEP75 = 1.67\ \sigma, \\ &CEP90 = 2.15\ \sigma, \\ &CEP95 = 2.45\ \sigma. \end{aligned} \tag{A9}$$

Bivariate Gaussian Distribution

Consider now a more general bivariate Gaussian distribution, that includes biases and unequal variances. The PDF can be written as

$$f_{X,Y}(x,y) = \frac{1}{2\pi\sigma_x\sigma_y} e^{-\frac{1}{2}\left(\frac{(x-\mu_x)^2}{\sigma_x^2}+\frac{(y-\mu_y)^2}{\sigma_y^2}\right)}, \tag{A10}$$

where

$$\begin{aligned} &\mu_x = \text{mean, or bias, of the } x \text{ variable}, \\ &\mu_y = \text{mean, or bias, of the } y \text{ variable}, \\ &\sigma_x^2 = \text{variance of the } x \text{ variable, and} \\ &\sigma_y^2 = \text{variance of the } y \text{ variable}. \end{aligned} \tag{A11}$$

We have arranged this distribution so that there is symmetry about the x and y axes. This implies that there is no correlation between x and y variables.

We now define functions of the x and y variables as

$$\begin{aligned} &r = \sqrt{x^2+y^2}\ , \text{ and} \\ &\theta = \text{atan}(y,x), \end{aligned} \tag{A12}$$

where the atan( ) function is a 4-quadrant arctangent, such that

$$\begin{aligned} &x = r\cos(\theta), \text{ and} \\ &y = r\sin(\theta). \end{aligned} \tag{A13}$$

Consequently, the CDF as the radius of interest increases is written as

$$CDF\left(r_0\right)=\int_0^{r_0}\int_0^{2\pi} f_{X,Y}\left(x,y\right)rd\theta dr\,, \tag{A14}$$

Ignoring for the moment the actual calculation of this, Eq. (A7) still holds, repeated here as

$$CEPxx=r_0 \quad \text{such that } CDF\left(r_0\right)=\frac{xx}{100}. \tag{A15}$$

Expanding Eq. (A14) yields

$$CDF\left(r_0\right)=\int_0^{r_0}\int_0^{2\pi}\frac{1}{2\pi\sigma_x\sigma_y}e^{-\frac{1}{2}\left(\frac{\left(r\cos\theta-\mu_x\right)^2}{\sigma_x^2}+\frac{\left(r\sin(\theta)-\mu_y\right)^2}{\sigma_y^2}\right)}rd\theta dr\,, \tag{A16}$$

for which it isn't quite as easy to find a general analytical solution as we might hope. Often these are calculated by numerical integration, although sometimes they can be reduced in complexity somewhat, say to a single integration.

<u>Biased PDF with Equal Variances</u>

For example, for a biased PDF, but otherwise equal variances, the CDF can be reduced to a single integration

$$CDF\left(r_0\right)\Big|_{\sigma_y=\sigma_x}=\int_0^{r_0}\frac{r}{\sigma_x^2}e^{-\frac{r^2+\mu_x^2+\mu_y^2}{2\sigma_x^2}}I_0\left(\sqrt{\frac{r^2\left(\mu_x^2+\mu_y^2\right)}{\sigma_x^4}}\right)dr\,, \tag{A17}$$

where

$$I_0\left(z\right)\text{ = modified Bessel function of the first kind.} \tag{A18}$$

<u>Zero-Mean PDF with Unequal Variances</u>

For a zero-mean PDF, but unequal variances, the CDF can be reduced to a single integration

$$CDF\left(r_0\right)\Big|_{\substack{\mu_x=0\\ \mu_y=0}}=\int_0^{r_0}\frac{r}{\sigma_x\sigma_y}e^{-\frac{r^2\left(\sigma_x^2+\sigma_y^2\right)}{4\sigma_x^2\sigma_y^2}}I_0\left(\frac{r^2}{4}\left(\frac{1}{\sigma_y^2}-\frac{1}{\sigma_x^2}\right)\right)dr\,. \tag{A19}$$

A plot of this in terms of CEPxx is given in Figure 15. Note that the column where $\sigma_y/\sigma_x=1$ corresponds to the examples in (A9). Note also that the radius that corresponds to a particular CEPxx decreases as the ratio σ_y/σ_x decreases. While it is intractable to directly calculate CEPxx, it is common to fit a simplified approximation to the contours in Figure 15.

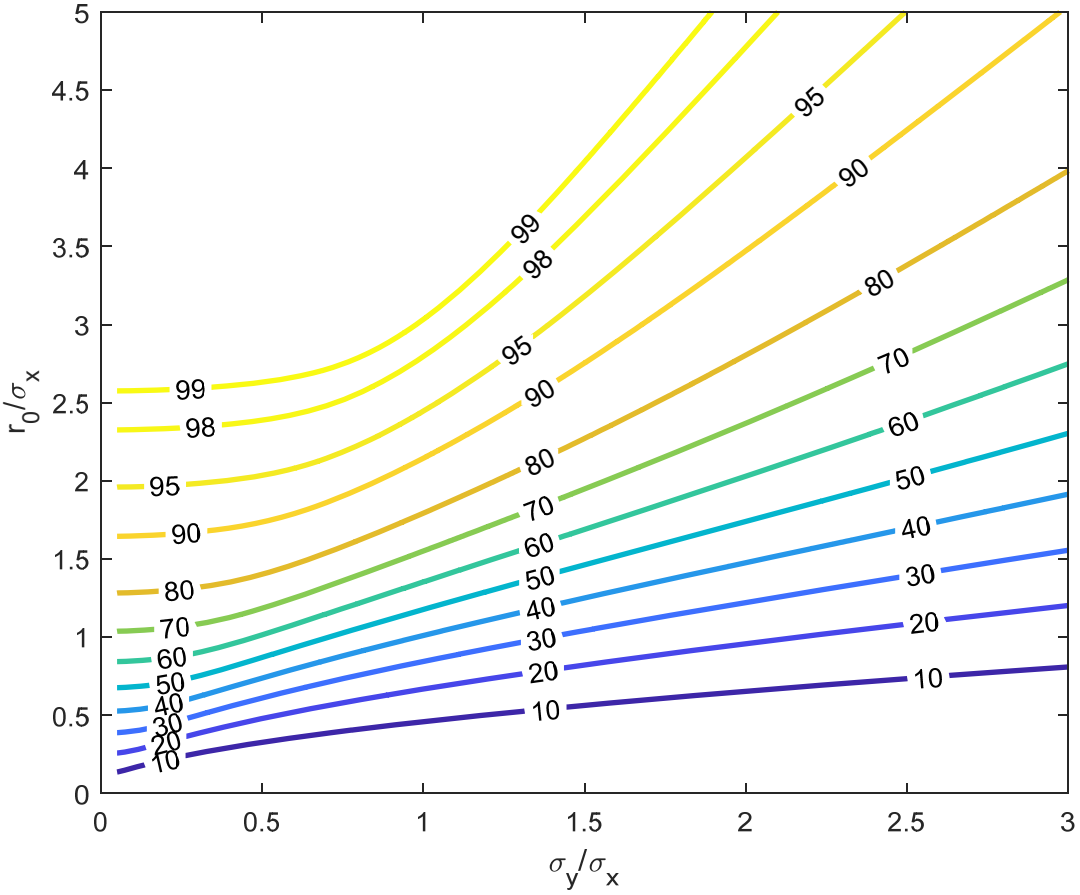

Figure 15. Plots of CEPxx curves (with contours labeled in xx) for zero-mean PDF, but unequal variances.

A common linear fit to the CEP50 contour is[21]

$$\frac{CEP50}{\sigma_x} = 0.6142\frac{\sigma_y}{\sigma_x} + 0.5632 \qquad \text{for CEP50, for } 0.3 \le \frac{\sigma_y}{\sigma_x} \le 1.0\,. \tag{A20}$$

The CEP90 contour is somewhat more curved, and hence might be better modelled with a polynomial. We offer the fit

$$\frac{CEP90}{\sigma_x} = -0.0643\left(\frac{\sigma_y}{\sigma_x}\right)^3 + 0.5564\left(\frac{\sigma_y}{\sigma_x}\right)^2 + 0.0588\left(\frac{\sigma_y}{\sigma_x}\right) + 1.6139\,, \qquad \text{for } 0.05 \le \frac{\sigma_y}{\sigma_x} \le 3.0\,. \tag{A21}$$

These simplified models are compared to numerically integrated contours in Figure 16. In both cases, better fits can be conjured if necessary.

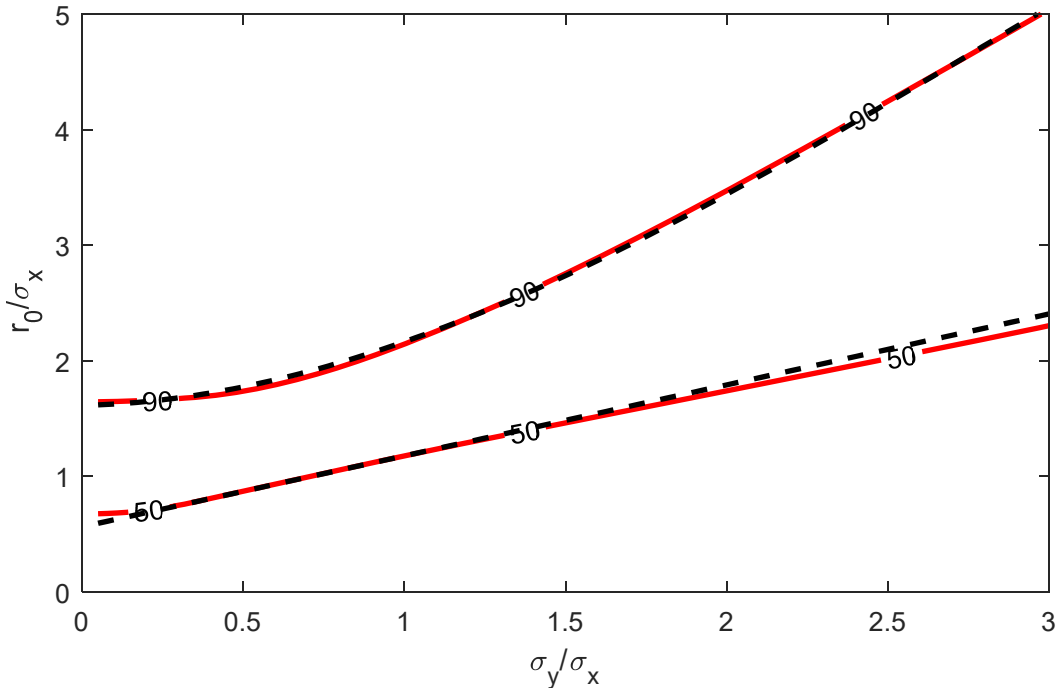

Figure 16. Curve fits to CEP50 and CEP90 contours. Solid red lines are numerically integrated contours. Dashed black lines are curve fits.

Biased PDF with Unequal Variances

We examine now a particular case where the PDF has unequal variances but an offset mean in the *y*-direction. This entails a numerical integration of Eq. (A16), repeated here

$$CDF\left(r_0\right)=\int_0^{r_0}\int_0^{2\pi}\frac{1}{2\pi\sigma_x\sigma_y}e^{-\frac{1}{2}\left(\frac{\left(r\cos\theta-\mu_x\right)^2}{\sigma_x^2}+\frac{\left(r\sin(\theta)-\mu_y\right)^2}{\sigma_y^2}\right)}rd\theta dr\,, \tag{A22}$$

but now allowing only $\mu_x=0$. This new degree of freedom will cause us to fix another aspect of the equation, which we choose to be the CEPxx. Specifically, now we wish to find the radius r_0 that equates to a particular CEPxx so that

$$\int_0^{r_0}\int_0^{2\pi}\frac{1}{2\pi\sigma_x\sigma_y}e^{-\frac{1}{2}\left(\frac{\left(r\cos\theta-\mu_x\right)^2}{\sigma_x^2}+\frac{\left(r\sin(\theta)-\mu_y\right)^2}{\sigma_y^2}\right)}rd\theta dr=\frac{xx}{100}\,, \tag{A23}$$

and do so for variations in σ_y/σ_x and μ_y/σ_x. Calculations of Eq. (A23) for CEP90 and CEP50 are shown in Figure 17 and Figure 18 respectively. Note that as the bias μ_y increases, so too do the radii for CEP90 and CEP50.

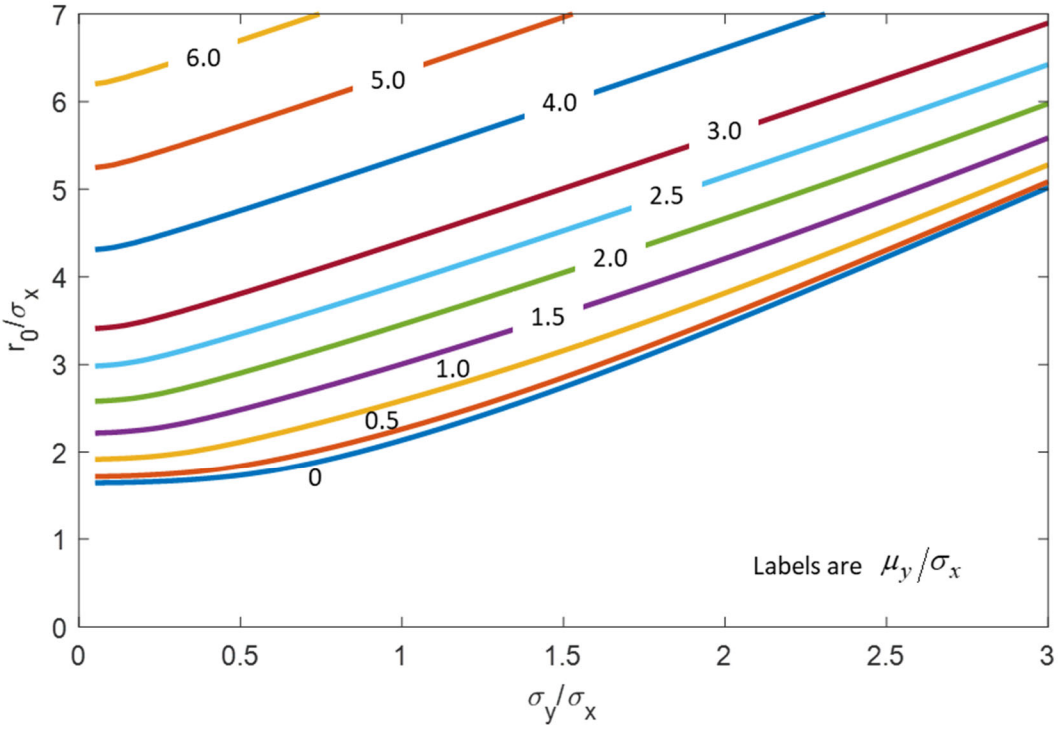

Figure 17. CEP90 contours for various bias offsets.

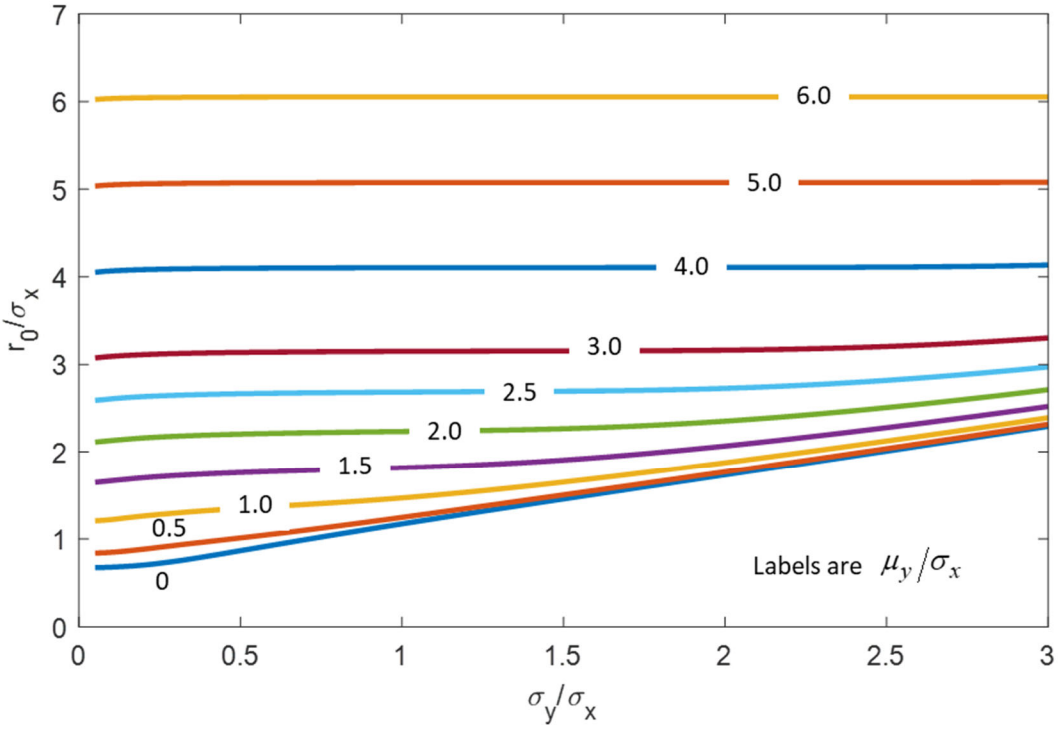

Figure 18. CEP50 contours for various bias offsets.

Appendix B – GPS Data Analysis

Here we present the results of an analysis of 86,789 GPS position samples collected at 1-second intervals with a NovAtel Flex Pak 6 receiver. The raw position offset readings are illustrated in Figure 19. The mean of Differential-GPS (DGPS) readings was considered "truth."

The L1 C/A code GPS data was segmented into observation intervals of some specific length, and then statistics calculated for each interval, and then averaged over all intervals of that same length. This was then repeated for a new interval length. These interval lengths correspond to synthetic aperture lengths of interest. Statistics were calculated separately for northing and easting. Figure 20 through Figure 23 show various statistics for intervals out to 3600 seconds. Recall that for our purposes we are interested in interval length from several seconds to low single-digit hundreds of seconds.

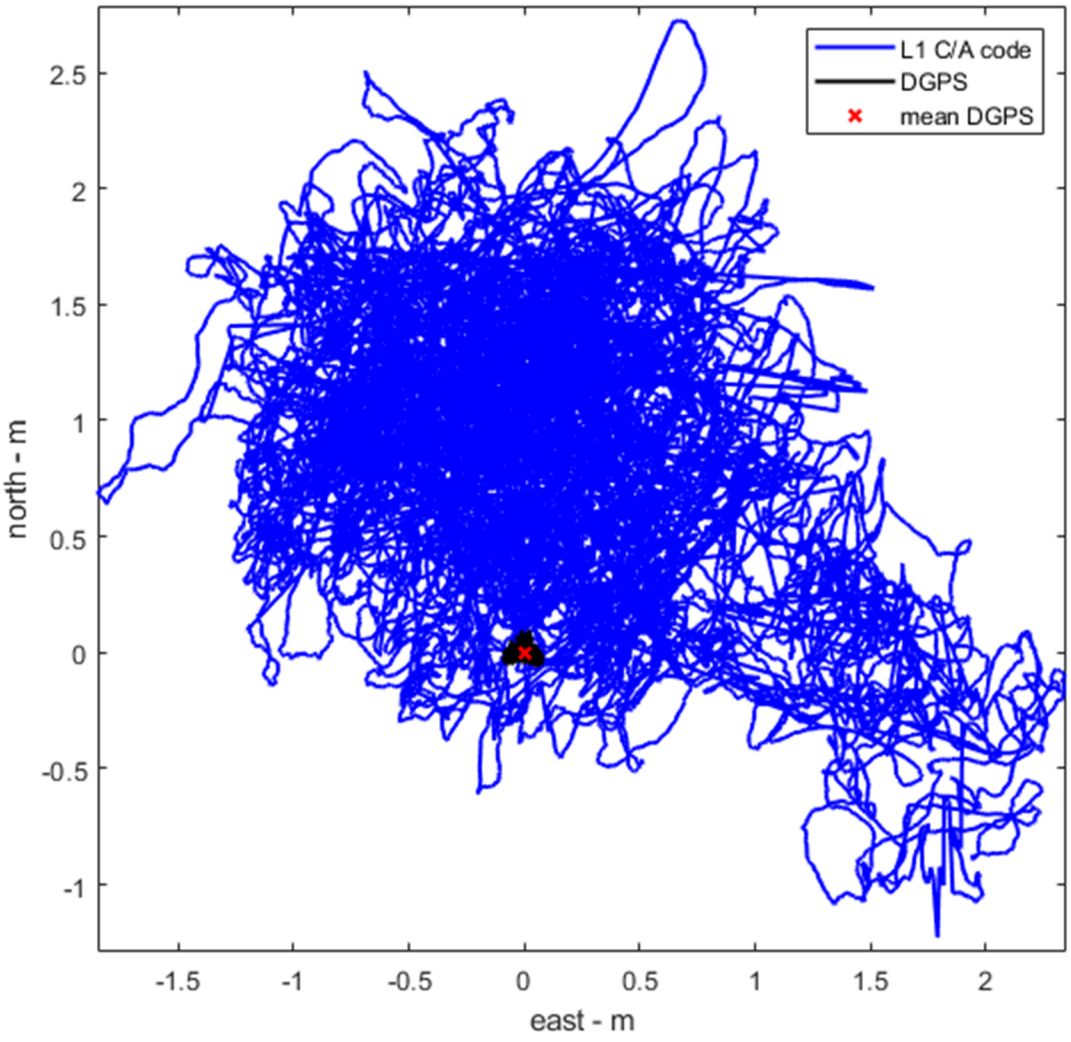

Figure 19. Position error calculations based on 86,789 sequential NovAtel Flex Pak 6 GPS receiver position readings. The mean of the DGPS offsets was considered "truth."

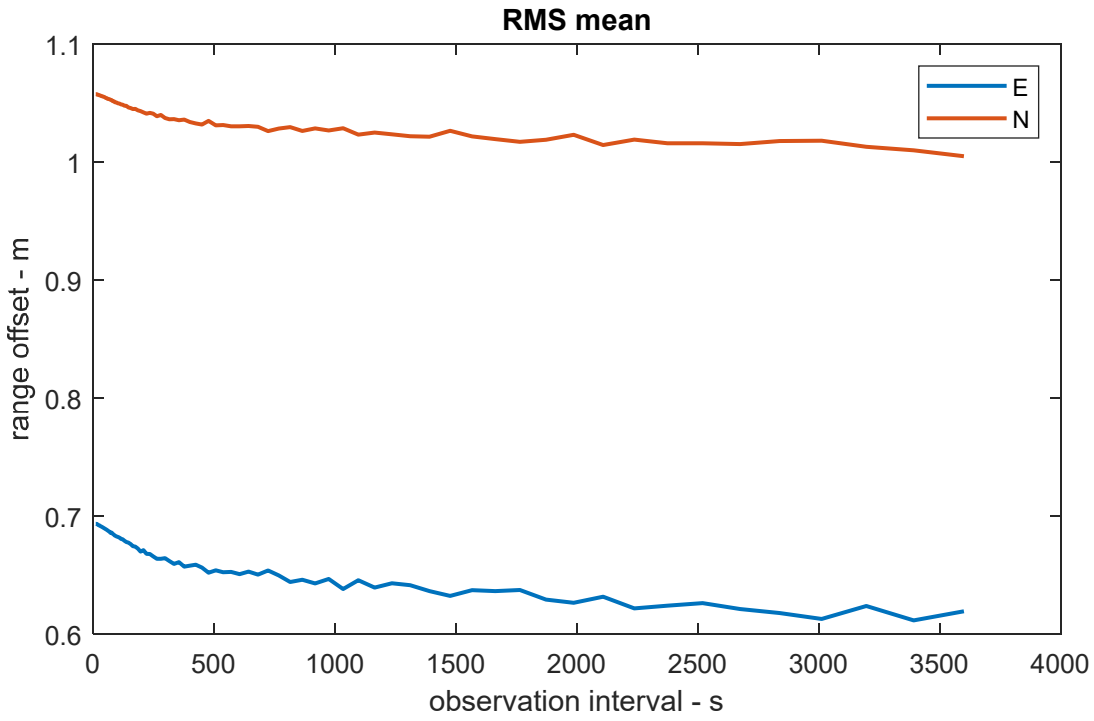

Figure 20. The mean is calculated for each interval, and then the RMS of the results.

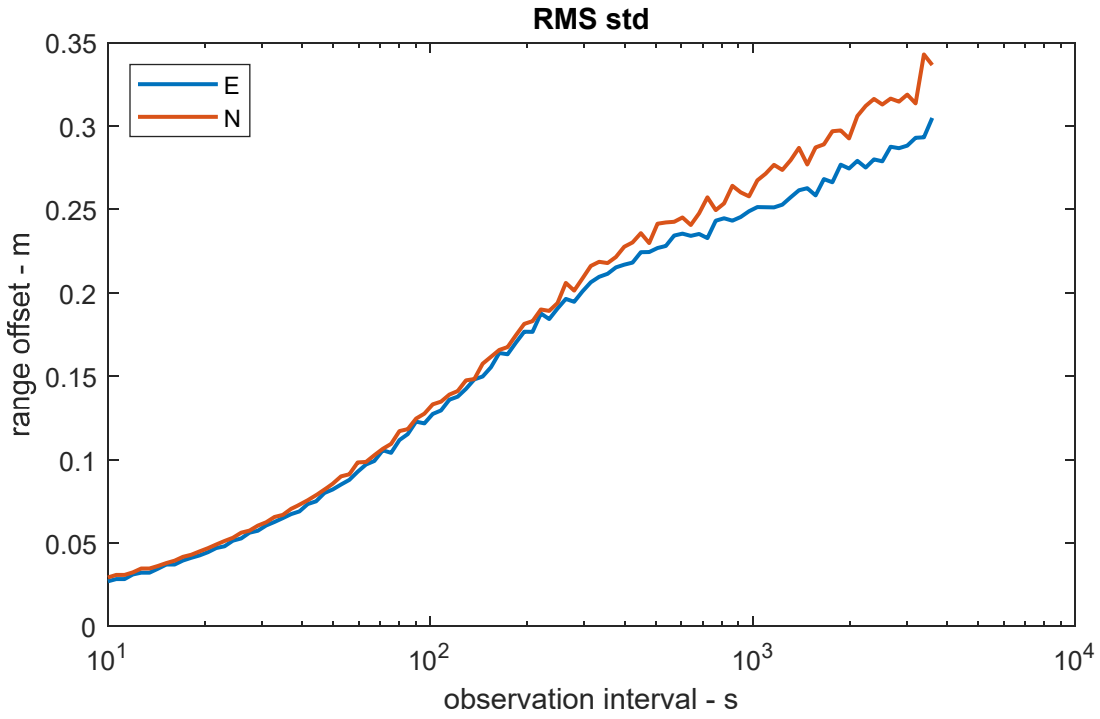

Figure 21. The standard deviation is calculated for each interval, and then RMS of the results. As the observation interval increases, more drifting is included in the standard deviation calculation.

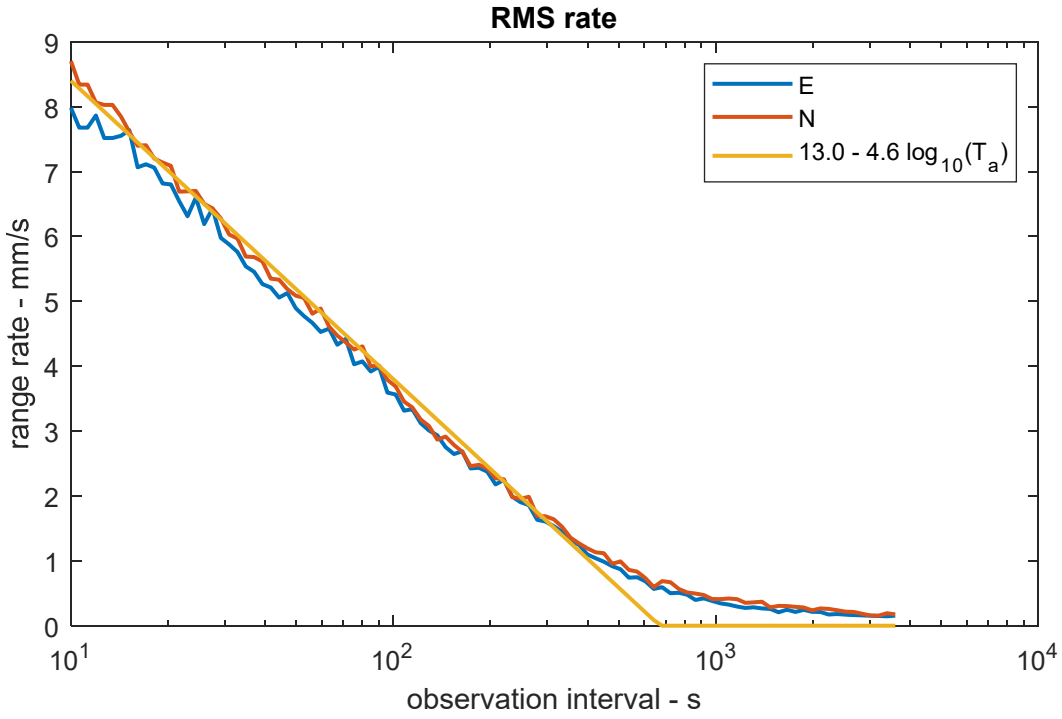

Figure 22. A linear fit is calculated to each interval, and then the RMS of the slope. Basically, a longer bounded offset will allow a lesser linear slope. Also plotted is a linear fit to the RMS range-rates.

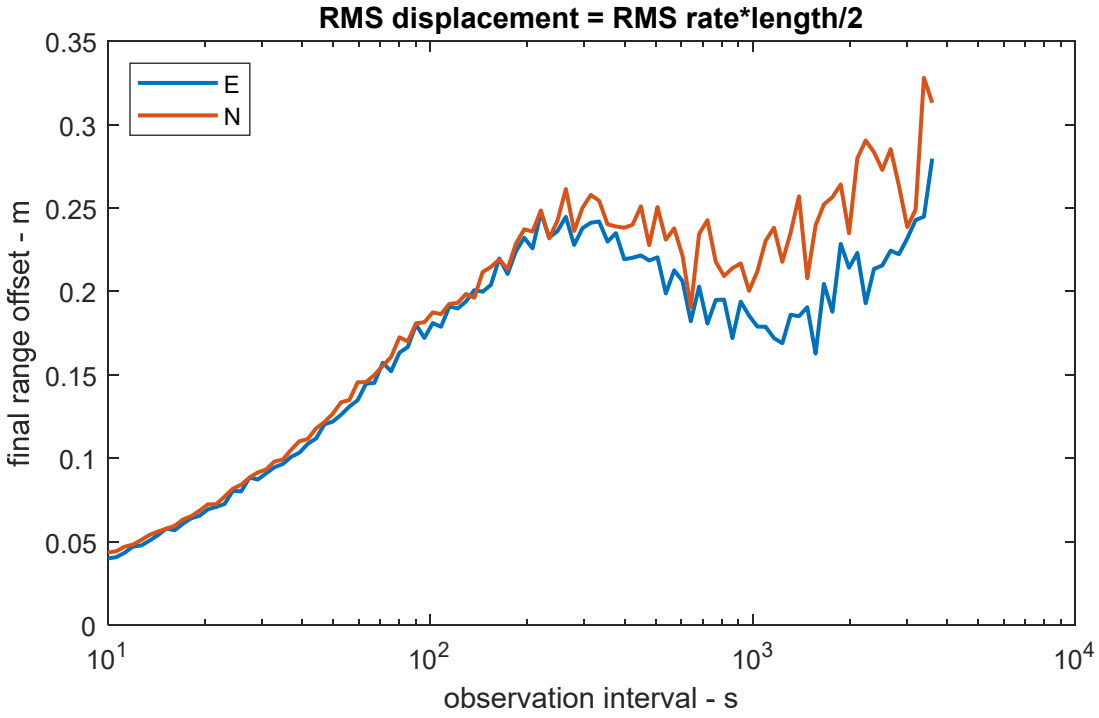

Figure 23. Given the linear range-rate of the previous slide, how much does the displacement change from the mean at the end of the observation interval? Longer observation intervals allow more drifting, to a point.

“If you torture the data long enough, it will confess.”
— Ronald H. Coase, Essays on Economics and Economists

Appendix C – Geolocation Error Categories

Geolocation is often characterized into categories based on error probabilities. From Joint Publication 3-09.3 we identify the following horizontal geolocation error categories.[22]

Table 4. Geolocation Error Categories.

Geolocation Error Category	*CEP 90*
I	0-6 m
II	7-15 m
III	16-30 m
IV	31-91 m
V	92-305 m
VI	> 305 m

“I've said for many, many years, as long as I can ever remember, when I'm asked,
'Hey, what do you look for first in a quarterback?'
The first thing I look for is accuracy, because the rest of it doesn't matter.
-- Troy Aikman

References

[1] D. N. Pedlar, D. J. Coe, "Target geolocation using SAR," *IEE Proceedings - Radar Sonar and Navigation*, Vol. 152, No. 1, pp. 35-42, February 2005

[2] Theodore J. Kim, J. Rick Fellerhoff, Steward M. Kohler, "An Integrated Navigation System Using GPS Carrier Phase for Real-Time Airborne/Synthetic Aperture Radar (SAR)," *Navigation – Journal of the Institute of Navigation*, Vol. 48, Issue 1, pp. 13-24, Spring 2001.

[3] William J. Hughes Technical Center WAAS T&E Team, *Global Positioning System (GPS) Standard Positioning Service (SPS) Performance Analysis Report*, submitted to Federal Aviation Administration GPS Product Team, Report #96, January 31, 2017.

[4] Brent A. Renfro, Miquela Stein, Nicholas Boeker, Emery Reed, Eduardo Villalba, *An Analysis of Global Positioning System (GPS) Standard Positioning Service (SPS) Performance for 2018*, Report TR-SGL-19-02, NAVSEA Contract N00024-17-D-6421, Task Order: 5101192, March 13, 2019.

[5] Armin W. Doerry, *Motion Measurement for Synthetic Aperture Radar*, Sandia National Laboratories Report SAND2015-20818, Unlimited Release, January 2015.

[6] Armin W. Doerry, *Performance Limits for Synthetic Aperture Radar – second edition*, Sandia National Laboratories Report SAND2006-0821, Unlimited Release, February 2006.

[7] Zoran Sjanic, Fredrik Gustafsson, "Navigation and SAR focusing with map aiding," *IEEE Transactions on Aerospace and Electronic Systems*, Volume 51, Issue 3, pp. 1652-1663, July 2015.

[8] C. J. Carter, "H_2S: An Airborne Radar Navigation and Bombing Aid*," Journal of the Institution of Electrical Engineers - Part IIIA: Radiolocation*, Volume 93, Issue 2, pp. 449-467, 1946.

[9] Armin W. Doerry, *Radar Range Measurements in the Atmosphere*, Sandia National Laboratories Report SAND2013-1096, Unlimited Release, February 2013.

[10] Armin W. Doerry, *Just Where Exactly is the Radar? (a.k.a. The Radar Antenna Phase Center)*, Sandia National Laboratories Report SAND2013-10635, Unlimited Release, December 2013.

[11] Armin W. Doerry, Douglas L. Bickel, *Phase Centers of Subapertures in a Tapered Aperture Array*, Sandia National Laboratories Report SAND2015-9566, Unlimited Release, October 2015.

[12] Mark A. Richards, "A Beginner's Guide to Interferometric SAR Concepts and Signal Processing," *IEEE A&E Systems Magazine*, Vol. 21, No. 6, pp. 5-29 June 2006.

[13] John DeLaurentis, Doug Bickel, *Multi-Phase-Center IFSAR*, Sandia National Laboratories Report SAND2005-8018, Unlimited Release, January 2006.

[14] Armin W. Doerry*, 3-D Target Location from Stereoscopic SAR Images*, Sandia National Laboratories Report SAND99-2643, October, 1999.

[15] John M. DeLaurentis, Armin W. Doerry, *Stereoscopic Height Estimation from Multiple Aspect Synthetic Aperture Radar Images*, Sandia National Laboratories Report SAND2001-2585, August 2001.

[16] "Implementation Profile for High Resolution Elevation (HRE) Products," Version 1.0, NGA Standardization Document NGA.IP.0002_1.0, 23 October 2009.

[17] Tom G. Farr, Paul A. Rosen, Edward Caro, Robert Crippen, Riley Duren, Scott Hensley, Michael Kobrick, Mimi Paller, Ernesto Rodriguez, Ladislav Roth, David Seal, Scott Shaffer, Joanne Shimada, Jeffrey Umland, Marian Werner, Michael Oskin, Douglas Burbank, Douglas Alsdorf, "The Shuttle Radar Topography Mission," *Reviews of Geophysics*, Vol. 45, No. 2, June 2007.

[18] https://www.usgs.gov/

[19] Fred M. Dickey, Armin W. Doerry, Louis A. Romero, "Degrading effects of the lower atmosphere on long range airborne SAR imaging," *IET Proceedings on Radar, Sonar & Navigation*, Vol. 1, No. 5, pp. 329–339, October 2007.

[20] *IEEE Standard Radar Definitions*, IEEE Std 686-2008, IEEE Aerospace and Electronic Systems Society, Sponsored by the Radar Systems Panel, 21 May 2008.

[21] George R. Pitman (editor), *Inertial Guidance*, ASIN: B0006AXOTI, John Wiley & Sons, 1962.

[22] "Close Air Support," (formerly "Joint Tactics, Techniques, and Procedures for Close Air Support"), Joint Publication 3-09.3, 08 July 2009.

“Keep it Simple, Stupid” (the KISS principle)
-- Clarence "Kelly" Johnson

Distribution

Unlimited Release

Email—External

Brandeis Marquette	Brandeis.Marquette@ga-asi.com	General Atomics ASI
Jean Valentine	Jean.Valentine@ga-asi.com	General Atomics ASI
John Fanelle	John.Fanelle@ga-asi.com	General Atomics ASI

Email—Internal

all members	534x	
Technical Library	9536	libref@sandia.gov

Sandia National Laboratories is a multimission laboratory managed and operated by National Technology & Engineering Solutions of Sandia LLC, a wholly owned subsidiary of Honeywell International Inc. for the U.S. Department of Energy's National Nuclear Security Administration under contract DE-NA0003525.